AEDC-TR-70-172

Copy 2



# EXPERIMENTAL INVESTIGATION OF THE SCATTERING OF A NITROGEN AERODYNAMIC MOLECULAR BEAM FROM A SOLID NITROGEN SURFACE

Frederick Arnold, M. R. Busby, and Ronald Dawbarn

ARO, Inc.

October 1970



VON KÁRMÁN GAS DYNAMICS FACILITY

ARNOLD ENGINEERING DEVELOPMENT CENTER

AIR FORCE SYSTEMS COMMAND

ARNOLD AIR FORCE STATION, TENNESSEE

PRODUCED FOR THE AIR FORCE

UNDER CONTRACT F40600-71-C-0002

# NOTICES

When U. S. Government drawings specifications, or other data are used for any purpose other than a definitely related Government procurement operation, the Government thereby incurs no responsibility nor any obligation whatsoever, and the fact that the Government may have formulated, furnished, or in any way supplied the said drawings, specifications, or other data, is not to be regarded by implication or otherwise, or in any manner licensing the holder or any other person or corporation, or conveying any rights or permission to manufacture, use, or sell any patented invention that may in any way be related thereto.

Qualified users may obtain copies of this report from the Defense Documentation Center.

References to named commercial products in this report are not to be considered in any sense as an endorsement of the product by the United States Air Force or the Government.

# EXPERIMENTAL INVESTIGATION OF THE SCATTERING OF A NITROGEN AERODYNAMIC MOLECULAR BEAM FROM A SOLID NITROGEN SURFACE

Fred Arnold, M. R. Busby, and Ronald Dawbarn
ARO, Inc.

## FOREWORD

The research reported herein was sponsored by the Arnold Engineering Development Center (AEDC), Air Force Systems Command (AFSC), Arnold Air Force Station, Tennessee, in support of Program Element 61102F, Project 8951.

The results of the research were obtained by ARO, Inc. (a subsidiary of Sverdrup & Parcel and Associates, Inc.), contract operator of the AEDC, AFSC, under Contract F40600-71-C-0002. The research was conducted from December 1969 to January 1970 under ARO Project SW3003. The manuscript was submitted for publication on May 22, 1970.

This technical report has been reviewed and is approved.

Michael G. Buja
1Lt, USAF
Research and Development Division
Directorate of Technology

Harry L. Maynard
Colonel, USAF
Director of Technology

## ABSTRACT

An aerodynamic molecular beam and phase sensitive detection system were used to investigate the spatial distributions of nitrogen molecules scattered from solid nitrogen for (1) incident beam energies of 0.44 ev [source stagnation temperature ($T_o$) = 1440°K] to 0.88 ev ($T_o$ = 2760°K), (2) incident angles (with respect to surface normal) of 30 to 70 deg, and (3) a surface temperature of 23°K. Highly lobular reflected distributions centered 15 deg from the surface opposite the incident beam were observed with position and shape independent of incident energy and angle. The capture coefficient decreased sharply with increasing beam energy and incident angle from normal. A limited investigation of a nitrogen-argon mixture was also undertaken. The reflected spatial distributions for the components were similar to those observed for the individual pure gases. A seeding effect in the expansion was observed to accelerate the heavier gas. Transient effects were also investigated. Initial capture coefficient for a clean surface was near unity but decreased to the steady-state value after a period of frost buildup. Beam interruption after frost buildup resulted in a trend toward the data observed with no previous cryodeposit. On beam resumption initial capture coefficient was high, then decreased to the steady-state value, with the effect dependent on time of beam interruption.

## CONTENTS



## APPENDIX
### Illustrations

Figure Page

# SECTION I
# INTRODUCTION

## 1.1 STATEMENT OF THE PROBLEM

An understanding of the interaction of high temperature rarefied gases with surfaces, particularly surfaces at temperatures less than the gas condensation temperature, is required for design of facilities for high altitude rocket plume testing. For design and use of such a facility, basic information is needed in the following areas: (1) distribution and temperature of reflected gases from both condensing and noncondensing surfaces, (2) capture coefficients for condensing surfaces, and (3) effects of gas mixtures.

This investigation is directed toward the interaction of nitrogen gas with surfaces maintained below the condensation temperature for nitrogen ($N_2$) (28°K at $10^{-5}$ torr).

## 1.2 BACKGROUND

A considerable amount of experimental work has been carried out on macroscopic aspects of gas-surface interactions (Refs. 1, 2, and 3). However, molecular beam techniques offer a capability for examining these processes on a near-microscopic basis, since background pressures of less than $10^{-7}$ torr provide mean free paths greater than the chamber diameter. Molecules that have reacted with the surface are thus unaffected by the background pressure, and recently developed instrumentation techniques utilizing ion gages and mass spectrometers may be used to evaluate the properties of the reflected gas. Stickney (Ref. 4) has provided an excellent description of molecular beam techniques, instrumentation, experimental results, and gas-surface theory through 1966.

A molecular beam chamber has been developed at AEDC (Ref. 5) along with instrumentation and techniques for modulated beam detectors (Ref. 6) and velocity distribution measurements (Refs. 7 and 8).

These facilities and techniques are currently being used in a series of investigations of basic gas-surface interactions at conditions closely approximating the interactions of rocket exhaust gases with the cryopump in a rocket plume test chamber. Hydrogen gas ($H_2$) is the rocket exhaust product most difficult to pump, and therefore most efforts have been directed toward hydrogen pumping. However, since hydrogen is likewise difficult to investigate in a molecular beam chamber, initial investigations have been directed toward other gases to obtain general information on cryopumping phenomena. A further reason for investigating gases other than hydrogen is that the currently feasible hydrogen pumping methods (cryosorption and cryopumping) require protection from gases other than hydrogen and precooling of the incoming high temperature hydrogen. Studies of gas surface interactions of nitrogen, then, are directly related to the hydrogen pumping geometrical arrangement and qualitatively related (since nitrogen and hydrogen are both diatomic) to the cryopumping of hydrogen.

Heald and Brown (Ref. 9) investigated condensation of room temperature gases (carbon dioxide ($CO_2$), nitrogen ($N_2$), and argon (Ar)) on cryogenic surfaces and also observed reflected patterns from noncondensing surfaces. Capture coefficients near unity were observed for condensing surfaces, and cosine reflected distributions were observed from noncondensing surfaces. Caldwell, Busby, and Brown (Ref. 10) reported lobular scattering patterns from a copper noncondensing target for incident gas temperatures of 1400 to 2500°K. Busby and Brown (Ref. 11) have recently investigated capture coefficient variations and reflected spatial distributions for argon at temperatures from 1400°K to 2300°K impinging on condensing surfaces. A significant decrease in capture coefficient with increasing beam temperature and angle of incidence was found. Further, the reflected distribution was highly lobular and the lobe center was near the surface regardless of the angle of incidence. Busby, Haygood, and Link (Ref. 12) have devised a hard-sphere scattering model which correlates the data observed in Ref. 11 for argon.

## 1.3 SCOPE OF THE INVESTIGATION

The objectives of this investigation were as follows:

1. To investigate the reflected spatial distributions and capture coefficients of high temperature nitrogen beams impinging on condensing surfaces.

2. To investigate time dependence of capture coefficient and reflected spatial distribution for nitrogen impinging on a condensing surface without a previous cryodeposit.

3. To make a preliminary investigation of the effects of a binary gas mixture on distribution of reflected nitrogen.

# SECTION II
# EXPERIMENTAL APPARATUS

## 2.1 AERODYNAMIC MOLECULAR BEAM CHAMBER

The aerodynamic molecular beam experimental test cell (Fig. 1, Appendix) is a stainless steel cylinder, 3 ft in diameter by 6.5 ft in length, which is subdivided into three sections by two removable bulkheads. The first bulkhead separates the nozzle section of the cell from the collimation section and serves as a mounting base for the beam skimmer. The beam collimating orifice is mounted on the second bulkhead which separates the collimation and test sections of the cell. The beam system and its performance have been previously presented by Brown and Heald (Ref. 5).

### 2.1.1 Nozzle Section

Vacuum conditions were produced and maintained in the nozzle section by a 16-in. oil diffusion pump, a 20°K gaseous-helium (GHe)-cryoliner, and a 77°K liquid-nitrogen ($LN_2$)-cooled cryoliner. The total pumping speed for air was in excess of 500,000 liters/sec. Operating pressures from $10^{-4}$ to $10^{-7}$ torr were maintained in this section.

The aerodynamic molecular beam source (Fig. 2) was mounted in the nozzle section of the cell. The source was a 1/4-in.-diam by 6-in.-long rhenium tube mounted in a water-cooled copper heat shield. The gas entered both ends of the source and flowed from a 0.0135-in.-diam orifice drilled through the 0.010-in. tube wall. Rhenium may be resistance-heated to temperatures of approximately 3000°K, although the highest gas temperature attained in these experiments was 2760°K. The gas temperature was determined by an optical pyrometer which was calibrated using gas temperatures obtained from the velocity distribution measurements (Section 5.2.2). For a given stagnation pressure and indicated pyrometer reading, gas stagnation temperature ($T_o$) was known in terms of incident beam energy ($E_i$).

It was discovered that at high temperatures the rhenium source was extremely vulnerable to oxygen impurities in the test gas. Therefore, a resistance-heated gas purifier filled with copper shavings was used to ensure oxygen-free test gas, and a vacuum pump was used to purge the source lines before establishing flow.

### 2.1.2 Collimation Section

An operating pressure of $< 10^{-7}$ torr was maintained in the collimation section by a 10-in. oil diffusion pump and the gaseous-helium- and liquid-nitrogen-cooled cryoliners. The pumping speed for air was in excess of 350,000 liters/sec in this section.

A small stream tube of the free jet expansion in the nozzle section was separated from the general flow field by a cryogenically cooled skimmer located at the entrance of the collimation section. The skimmer was a hollow copper cylinder (Fig. 2) with a 1-in.-diam hole which allowed passage of the gas into the section. Gaseous helium at 20°K was circulated within the cylinder which cryopumped a portion of the impinging free jet expansion. The cooled skimmer was developed by Ruby (Ref. 13) and virtually eliminated the interaction previously reported by Brown and Heald (Ref. 5). At the end of the collimation section a 4-mm-diam orifice, aligned with the skimmer and nozzle orifice, collimated the gas stream so that a uniformly intense and monoenergetic molecular beam entered the test section.

### 2.1.3 Test Section

In the test section vacuum conditions were maintained by a 10-in. oil diffusion pump and the 20°K gaseous helium and 77°K liquid-nitrogen-cooled cryoliners; the pumping speed for air was in excess of 110,000 liters/sec. An operating pressure of $< 10^{-7}$ torr was maintained in this section, which contained the beam detection systems, the cryogenically cooled target, and their mounting and drive mechanisms.

## 2.2 DETECTION SYSTEMS

The use of molecular beams for atomic and molecular interaction experiments has resulted in the development of several practical beam detection techniques (Ref. 14). One technique which aids in the discrimination between the beam signal and background noise is to modulate the molecular beam at a convenient frequency and then by AC amplification measure only that part of the signal which has the proper frequency and

phase. This is generally referred to as modulated-beam or lock-in detection, and the technique is described in detail in Refs. 15 and 16. The detector system described herein combines the beam modulation technique with a quadrupole mass spectrometer as the electrical signal source. The use of the mass spectrometer further increases the signal-to-noise ratio of the detector by rejecting all signals at mass numbers other than the beam mass number.

The detector was designed for two modes of operation: (1) as a molecular flow rate detector and (2) as a number density detector. The mode of operation is determined by the manner in which the beam gas is introduced into the detector ionization region as shown in Fig. 3. As a molecular flow rate (beam intensity) detector, the beam must pass into the steady-state box before entering the ionization region of the mass spectrometer. Since the beam molecules are brought to equilibrium with the walls and the baffle of this box, the detector responds only to changes in number density within the box, which is in turn proportional to molecular flow rate. All spatial flux distribution data were taken in this operational mode. The box is removable to permit use of the instrument as a flow density detector. In this configuration the beam pulses pass directly through the ionization region without striking any solid surface, and the rate of ionization is proportional to the number density of the beam gas in the ionization region. The time-of-flight or beam energy measurements (Section 5.2.2) were made in this operational mode.

The detector arrangement for the spatial distribution mode is depicted in Fig. 4. The molecular beam to be detected is chopped into pulses by two slots in a rotating wheel. These slots are 90-deg sectors cut out of a 2-in.-diam aluminum disk. The beam chopper is turned by a two-phase, synchronous, vacuum-rated motor driven at 150 Hz. These beam pulses then pass into the ionization region of the quadrupole mass spectrometer which is tuned to the mass number of the beam molecules. The resulting ion current is amplified by an electron multiplier which sends a pulsed electrical signal to the lock-in amplifier. This amplifier operates as a narrow bandpass amplifier, the center frequency of which is adjusted to the chopping frequency. The amplifier increases the signal-to-noise ratio by amplifying only the electrical signals within this small frequency range. The signal-to-noise ratio is further increased by rectifying the amplifier output with a switching circuit driven by a reference signal from a light and photocell at the chopper. Thus, only signals with the exact chopping frequency are rectified. A manual phase-shift in the reference circuit is used to maximize output, and an adjustable resistance-capacitance (RC) circuit in the output is used for smoothing. The signal is read out on a strip-chart recorder, and an oscilloscope is used to monitor phasing and mass spectrometer output.

This detection system is capable of recovering beam intensity signals that are three orders of magnitude less than the background gas intensity. A complete description of the detectors and their performance has been given by Heald (Ref. 6).

The total beam flux (molecules/sec) was measured by a miniature ionization gage. The gage was enclosed in a glass envelope, but the normal 1-in.-diam opening was reduced

to 6 mm in order to increase the directional sensitivity (Fig. 1). Calibration of the gage in terms of beam flux was obtained by using an oven-type molecular beam to provide a known flux.

## 2.3 TARGET AND DETECTOR MOVEMENT MECHANISMS

The target and its mount rotated about an axis perpendicular to the incoming beam (Fig. 5). Motion was accomplished by a variable-speed motor with a chain drive. The position of the target was determined from a calibrated voltmeter readout which was produced from a ten-turn potentiometer connected to the chain drive. In-plane and out-of-plane motions (see Section III) were likewise provided by a torque-motor chain-drive combination (Fig. 5), and a potentiometer and voltmeter system was used to determine the position of the detector.

## 2.4 TARGET SUBSTRATE

The target substrate for these experiments was a copper disk hand-polished to a mirror finish with jeweler's rouge and rinsed with acetone. The disk is hollow so that gaseous helium can be circulated through it. The substrate temperatures were maintained by a Collins cryostat. Chromel®-constantan thermocouples were used to measure target temperatures in the range of 20 to 36°K.

# SECTION III
# DETECTOR MOVEMENT GEOMETRY AND COORDINATE SYSTEM

For a target-fixed coordinate system the incident beam unit vector, $\vec{i}$, is defined through an azimuthal angle, $\theta_i$, measured from the unit target normal, $\vec{n}$. The plane containing $\vec{n}$ and $\vec{i}$ will be referred to as the in-plane or principal plane (Fig. 6); the intersection of this plane with the target face will be referred to as the principal axis. The transverse axis is perpendicular to the principal axis and also lies on the target face.

The geometry used to describe the reflected beam is shown in Fig. 7. The reflected or scattering direction is denoted by the unit vector $\vec{r}$. The detector lies along the vector $\vec{r}$ at constant radius R. An out-of-plane or transverse plane is defined as that plane containing the transverse axis and the vector $\vec{r}$. Note that the transverse planes are always perpendicular to the principal plane. The line of intersection of a transverse plane with the principal plane makes an in-plane angle, $\theta_r$, with the target normal, $\vec{n}$, and an out-of-plane angle, $\phi$, with the reflection vector, $\vec{r}$. Since $\vec{r}$ is a variable, many transverse planes exist, all passing through the single transverse axis. Properties displayed in planes of constant $\theta_r$ are transverse sections of the scattered beam while a display of the properties in the plane, $\phi = 0$, is a principal plane section of the scattered beam. The coordinate system defined by $\theta_r$ and $\phi$ is a standard spherical coordinate system with $\theta_r$ the azimuthal or longitudinal angle and $\phi' = 90 - \phi$ the polar or co-latitude angle. The transverse axis corresponds to the polar axis.

## SECTION IV
## CAPTURE COEFFICIENT–CALCULATION PROCEDURE

The beam capture coefficient has been defined previously by Heald and Brown (Ref. 9) as

$$C_b = 1 - \frac{\dot{n}_r}{\dot{n}_i}$$

where $\dot{n}_r$ it the total reflected beam flux (molecules/sec) and $\dot{n}_i$ is the total incident beam flux. If any gas is evaporating from the target surface, the magnitude of the evaporation flux can be determined by extinguishing the incident beam and recording the remaining detector signal. Thus, the reflected beam flux is the difference between the total gas flux leaving the surface, $\dot{n}_t$, and the evaporation flux. In these experiments the surface temperatures, $T_s$, were such that the evaporation flux was not detectable. Therefore, the effective beam capture coefficient is

$$C_b = 1 - \frac{\dot{n}_t}{\dot{n}_i}$$

The phase-sensitive detection system responds to the number of particles per area per time at radius R, and thus the total reflected beam flux may be determined from the relation

$$\dot{n}_t = K \int_A S(\theta_r, \phi')\, dA = KR^2 \int_0^{\pi} \int_{-\pi/2}^{\pi/2} S(\theta_r, \phi') \sin \phi' \, d\theta_r \, d\phi'$$

where $S(\theta_r, \phi')$ is the detector signal, K is the detector calibration constant, and $\theta_r$ and $\phi'$ are the angles defined in Fig. 7. The total incident nitrogen flux, $\dot{n}_i$, is determined from the reference cosine distribution of the noncondensing beam on the 36°K copper substrate. Thus, $\dot{n}_i$ may be analytically determined since for a diffuse reflection (cosine distribution)

$$\dot{n}_i = \pi KR^2 S_{ref}$$

where $S_{ref}$ is the maximum signal intensity for the cosine distribution. If $\phi$ is substituted for $\phi'$ in the expression for $\dot{n}_t$, the beam capture coefficient may be expressed as

$$C_b = 1 - \frac{2}{\pi S_{ref}} \int_0^{\pi/2} \int_0^{\pi/2} S(\theta_r, \phi) \cos \phi \, d\phi \, d\theta_r$$

Symmetry about the principal plane is assumed. No reflected signals for $\theta_r < 0$ were observed for condensing target temperatures; therefore, $\theta_r$ is integrated from 0 to $\pi/2$. The calibration of the mass spectrometer enters only in the form of $S_{ref}$, the maximum signal intensity of a diffusely reflected beam of the same intensity. The integral expression was evaluated by a double integral Simpson's rule method on a digital computer. Transverse scattering plane data were recorded at 5-deg increments of $\theta_r$ over

the range of 30 to 90 deg. In each of the transverse planes, 5-deg increments of $\phi$ were taken from 0 to 45 deg. Thus, the three-dimensional lobular scattering patterns were placed on a grid of mesh size 5 by 5 deg. However, atoms scattered into regions of $\theta_r <$ 30 deg and $\phi >$ 45 deg were neglected since their contribution to the capture coefficient was observed to be negligible.

# SECTION V
# EXPERIMENTAL PRETEST PROCEDURES

## 5.1 SYSTEM ALIGNMENT AND CALIBRATION

The alignment of the skimmer, collimator, target, and detector system was accomplished by a laser beam. Following the calibration of the potentiometer-voltmeter system, the target could be positioned to within an estimated ±1 deg of arc, whereas the in-plane and out-of-plane angles were observed to be within an estimated ±1/2 deg of that indicated by a voltmeter reading. In addition to the electrical position indicator, reference marks for the target and detector positions in the test section were visually observed during these experiments as a check on the potentiometer calibrations.

## 5.2 BEAM CHARACTERISTICS

### 5.2.1 Intensity Cross Section of the Nitrogen Beam

Measurements were made with the miniature ionization gage (Section 2.2) to determine the intensity (molecules/sec-cm$^2$) at various points across the beam. A plate with a 0.35-mm-diam hole was placed over the ionization gage opening and readings were taken at positions visually measured with a transit. As shown in Fig. 8, the beam distribution has an approximately uniform core.

### 5.2.2 Nitrogen Beam Energy Measurements

In order to measure the incident nitrogen beam energy, $E_i$, the detector system was operated in its flow density or fly-through mode (Fig. 3). The velocity distributions for a constant source pressure (1500 torr) and variable source temperatures were obtained. The experimental apparatus and data acquisition procedures have been described in detail by Powell and Heald (Ref. 7). The reduction of the velocity distribution data is discussed by Benek, Busby, and Powell (Ref. 8). The normalized data and the corresponding best-fit theoretical distribution for a heated nitrogen beam are shown in Fig. 9. Beam energies determined from the velocity distribution data and their corresponding indicated source temperatures are presented in Fig. 10. The source temperatures were set with an optical pyrometer, and it was assumed throughout these experiments that the pyrometer reading would repeatably indicate the corresponding beam energy. The calculated stagnation temperatures are based on an assumed equilibrium conversion of stagnation enthalpy to the measured total translational energy, with variable specific heats. It should be pointed out, however, that the rotational and vibrational temperatures are probably not equal to the measured translational static temperatures because of the different locations of the respective frequency points in the jet.

The nitrogen molecular beam used in these experiments is a nearly monoenergetic aerodynamic molecular beam. Aerodynamic beams differ from classical oven or Maxwellian beams in several areas: (1) the intensity is greater, (2) the mean energy is higher, and (3) the velocity distributions are very narrow. The term monoenergetic is applied since at Mach 20, for example, the velocity distribution of an aerodynamic beam is such that 80 percent of the beam molecules have a velocity that is within five percent of the mean velocity (Ref. 17).

### 5.2.3 Nitrogen Beam Performance

Nitrogen beam performance data were obtained by lowering the miniature ionization gage into the beam and obtaining the gage reading as the source pressure, $P_o$, and temperature, $T_o$, were varied over the desired range (Fig. 11). Previous calibration of the ionization gage with an oven beam source had shown that if the ionization pressure gage reading for nitrogen was multiplied by $3.8 \times 10^{20}$ the result was the total beam flux in molecules per second.

## 5.3 VARIATIONS IN MASS SPECTROMETER SENSITIVITY

The variation of the mass spectrometer sensitivity with time was determined in the following manner:

1. An incident nitrogen beam of known intensity, $I_o$, and energy, $E_i$, was scattered from the 285°K copper target.

2. The detector was positioned at the target normal and all the electronics were activated.

3. The reflected molecule signal was maximized, and its value recorded as a function of time (Fig. 12).

After four hours of operation, the signal magnitude remained nearly constant as time increased. The variation of the signal was primarily attributed to a loss in sensitivity with time of the magnetic strip electron multiplier used to detect the quadrupole ion current.

Before the data were collected, the mass spectrometer was operated for approximately four hours with the beam reflected from a noncondensing target, thus assuring a relatively stable sensitivity for the experimental data. By periodically returning to the reference condition, sensitivity shifts could be detected.

## 5.4 TEST SECTION BACKGROUND PRESSURE

A mass spectrometer scan of the background gases in the test section revealed that water was the primary background constituent. The partial pressure of water was estimated to be $5 \times 10^{-9}$ torr which corresponds to a strike rate $2.4 \times 10^{12}$ molecules/sec-cm$^2$. A typical experimental nitrogen beam intensity, $I_o$, is $1.2 \times 10^{16}$ molecules/sec cm$^2$, and thus water accounts for 0.02 percent of the total number of molecules striking the target per second. For all experimental tests the total background gas pressure was in the range of $2.0$ to $3.0 \times 10^{-8}$ torr.

# SECTION VI
# EXPERIMENTAL PROCEDURE

## 6.1 SPATIAL DISTRIBUTIONS–STEADY STATE

The experimental procedures for obtaining reflected spatial distributions were as follows:

1. After pumpdown and cooldown of the chamber, the phase-sensitive detection system was activated and adjusted for proper sensitivity and resolution for nitrogen. The detector system was positioned on the target normal.

2. An unheated nitrogen beam was started and adjusted to provide an intensity of $1.95 \times 10^{16}$ molecules/sec-cm$^2$ as measured with the miniature ionization gage.

3. Cooldown of the target was initiated and the target was cooled to approximately 36°K (slightly above condensation temperature).

4. After allowing approximately four hours to attain constant mass spectrometer sensitivity, a reference reflected distribution was taken. These data provided a reference for the performance of the detector system as nitrogen does not condense on a 36°K surface, and the reflected spatial distributions are diffuse. A typical reference distribution is shown in Fig. 13.

5. After obtaining the reference distribution, the beam was stopped and the target cooled to the desired temperature (23°K in these experiments). The beam was then started and adjusted to the desired energy (source temperature) and intensity.

6. With the detection system positioned for the expected maximum reflected signal (in-plane, 75 deg from normal), the detector output was monitored until steady state was achieved, usually within 30 minutes.

7. After a steady-state condensation rate was achieved, spatial distributions of reflected nitrogen molecules were recorded in both the principal and transverse planes.

8. At the end of a set of experimental runs, the copper substrate was warmed to 36°K and the nitrogen cryofrost evaporated. A 285°K nitrogen beam was then scattered from the 36°K copper substrate, and the resulting cosine distribution was recorded. A comparison of this distribution with the one initially recorded revealed any changes in the detector system sensitivity.

## 6.2 SPATIAL DISTRIBUTIONS–TRANSIENT

In-plane spatial distributions were recorded during the buildup of cryodeposit on an initially clean surface. The experimental procedures were similar to the steady-state procedures except for data acquisition.

Data were taken for these experiments by setting the detector at a desired position with the output connected to a strip-chart recorder. The beam was started and adjusted to the desired energy and intensity with the target at 36°K (noncondensing). After blocking the beam from the target with the miniature ionization gage, the target was cooled to approximately 23°K. By simultaneously unblocking the beam and starting the recorder, transient buildup of reflected flux at one detector position could be recorded. The transient in-plane distributions were obtained by repeating this procedure at different positions for the same beam and target conditions.

# SECTION VII
# EXPERIMENTAL RESULTS AND DISCUSSION

## 7.1 DISTRIBUTION OF REFLECTED MOLECULES

Steady-state spatial distributions of reflected molecules were obtained for the following incident beam stagnation temperatures and incident angles from the target normal:

| | $\theta_i$, deg | | | |
|---|---|---|---|---|
| $T_o$, °K | 30 | 45 | 60 | 70 |
| 1440 | | | X | X |
| 1670 | | X | X | X |
| 2140 | X | X | X | X |
| 2380 | X | X | X | X |
| 2760 | | | X | |

Figure 14 exhibits the general configuration of all reflected steady-state distributions after normalizing with respect to maximum signal. Maximum reflected intensity occurred at approximately 75 deg from normal (15 deg from the surface), and this location was relatively insensitive to beam energy and angle of incidence. In the figure, distance from the origin is proportional to reflected flux at that angular position as measured at the constant detector position radius. It was necessary to assume symmetry about the principal plane, since only positions on one side of the principal plane were accessible. The slight increase in signal at small transverse angles (Fig. 14) was consistent for all cases, but may have been caused by movement and capacitance coupling of the mass spectrometer cables.

Although the general lobe shapes were similar for all conditions investigated, closer examination of the data reveals some differences. Figures 15 and 16 represent data taken in the principal plane, normalized with respect to the maximum signal. A slightly broader distribution may be noted with increased incident beam energy. Likewise, a

broader distribution results from decreasing the angle of beam incidence. In addition, there is a small dependence of angle of maximum reflection on beam energy and incidence angle. It should be noted that these changes would be less obvious on a polar plot.

The effects of beam intensity were not investigated in these experiments except for one case. Normally the intensity was $1.95 \times 10^{16}$ molecules/sec-cm$^2$, but one spatial distribution was taken at half of this value. As with argon (Ref. 11), no significant effect was observed.

The effects of target temperature were not investigated; all data were for a 23°K target temperature.

## 7.2 CAPTURE COEFFICIENT

As discussed in Section IV, the spatial distribution data may be integrated in conjunction with the reference cosine data to obtain the capture coefficient for the particular conditions. Results of these calculations are presented in Figs. 17 and 18. Capture coefficient is seen to decrease with increasing beam stagnation temperature (beam energy) and with increasing angle of incidence from normal. Beam incidence angles greater than 70 deg could not be investigated because the detector-target geometry allowed direct beam incidence into the detector at detector positions close to the surface. It should be emphasized that the preceding data are for steady-state conditions; that is, the nitrogen frost had built up at incident conditions until a steady-state reflected distribution was obtained. Transient effects are discussed in Section 7.4.

The two primary sources of error in the capture coefficient data are believed to be changing mass spectrometer sensitivity during a run and fluctuation of target temperature during a run. On several occasions, large step changes in sensitivity were observed which could not be explained, and data from such runs were discarded and the run was repeated. Smaller changes in sensitivity occurring during the test (between cosine references) but not during actual data taking may not have been detected. Thus the sensitivity during data taking would not be the average of the preceding and succeeding reference values, as was assumed for data reduction.

Although effects of target temperature were not investigated, the argon investigation (Ref. 11) indicates that the capture coefficient is affected by target temperature. The target temperature was set at 23°K using a thermocouple and was estimated to be accurate to within ±2°K.

In order to make estimates of capture coefficient without taking complete spatial distribution data, it was decided to utilize the shape similarity of the reflected lobes. To accomplish this, the parameter (1-C) ($S_{ref}/S_{max}$) was calculated from spatial distribution data and plotted versus temperature and angle of incidence (Fig. 19). In this parameter, (1-C) is the reflected flux fraction and $S_{ref}/S_{max}$ is the ratio of the cosine reference signal to the maximum observed reflected signal. The parameter may be considered as the normalized ratio of volume to length of the reflected distribution. Thus, an estimate of capture coefficient may be made from the ratio of the maximum reflected signal to the cosine reference signal.

## 7.3 COMPARISON WITH ARGON DATA

The nitrogen data reported herein exhibit identical behavior to the argon data reported in Ref. 11. The primary trends may be summarized as follows:

1. Highly lobular spatial distributions of reflected flux with the maximum flux approximately 15 deg from the surface.

2. Very slight dependence of lobe shape and location on incident beam temperature and angle of incidence.

3. Decrease in capture coefficient with increasing incident gas stagnation temperature.

4. Decrease in capture coefficient with increasing angle of incidence from target normal.

It is indeed surprising that trends (and approximate magnitudes) predicted by a hard sphere model (Ref. 12) for a monatomic gas impinging on its own solid phase will apply to a diatomic gas under similar circumstances. The implication may be drawn that at least for nitrogen, vibrational and rotational modes are not involved in the gas-surface interaction and further that the molecular force field is approximately spherical. In subsequent work, an attempt will be made to compare energy distributions of reflected molecules with the hard sphere model.

## 7.4 TRANSIENT EFFECTS

### 7.4.1 No Previous Cryodeposit

As has been noted in Section 6.1, a period of frost buildup is required to achieve a steady-state reflected distribution and steady-state capture coefficient. This transient buildup was investigated for one condition, 1670°K beam stagnation temperature and 60-deg angle of incidence, following the procedure outlined in Section 6.2. Results for the first 50 sec are shown in Fig. 20 and for 15 min after beam initiation in Fig. 21. No significant changes occurred after 15 min. The reflected distribution appears to be initially a sum of cosine and lobular distributions, but within 10 sec becomes more lobular, then slowly increases to the steady-state values. It is probable that surface preparation would affect the initial distribution, with a rough surface giving a higher initial capture. The estimated capture coefficient (reference Section 7.2) as a function of time is shown in Fig. 22. The test surface in these experiments was polished, but was inevitably coated with small amounts of $H_2O$ from the $10^{-8}$ torr test chamber background. For a beam intensity of $1.95 \times 10^{16}$ molecules/sec-cm$^2$, the frost coverage after 1000 sec would be $9 \times 10^{-4}$ gm/cm$^2$. For assumed average frost density of 0.9 gm/cm$^3$ the approximate frost thickness would be 10 microns or 0.0004 in.

Because of limited chamber availability, no other frost buildup experiments were accomplished. It was observed, however, that the time required to reach steady-state conditions was not constant for a given intensity (molecules/sec-cm), but varied with beam stagnation temperature and angle of incidence. Further, if a frost layer sufficient to achieve steady state was built up for a given set of incident conditions, readjustment to different incident conditions required very short adjustment times, particularly if the angle of incidence was not increased so that the area of the target covered by the beam was not increased. Thermal gradients through the frost must be ruled out, as continual deposition of frost would then be inconsistent with a steady-state reflected distribution. Future work may extend these data to other incident conditions.

### 7.4.2 Effect of Beam Interruption

An additional transient effect was observed when the beam was interrupted after having achieved steady-state capture. With the detector system located 75 deg from normal (where maximum reflected flux is expected), the signal after resumption of the beam showed an initial peak, a dip, then a slow rise toward the steady-state value. The results are shown in Fig. 23 for various periods of beam interruption. Signal buildup for a surface with no prior cryodeposit is shown for comparison. It is apparent that a change in surface properties of the cryodeposit occurs, with a trend toward the reflection buildup measured with no previous cryodeposit. The degree of recovery increases with increasing beam interruption. Since the capture coefficient decreases as reflected flux increases, the initial capture coefficient on beam resumption is higher than the steady-state value, except for the initial burst of reflected flux.

No satisfactory explanation can be given for the initial peak on beam resumption. Two possibilities are: (1) surface effects such as initial sputtering of the frost, and (2) temporarily increased mass spectrometer sensitivity during the beam interruption. Sputtering was investigated by Busby (Ref. 11) and found not significant, but the possibility of other surface effects cannot be ruled out. Mass spectrometer sensitivity changes seem most likely.

If the transient effects noted here and in the preceding paragraph are observed over the entire range of incident conditions, performance of cryopumps for short-duration tests will be considerably better than the steady-state data suggests. Thus, for short-duration tests, rocket plume test chambers may be capable of accommodating larger propellant mass flow rates than would be predicted from the steady-state data.

## 7.5 EFFECT OF MIXED GAS

Experiments were run to determine the effect of a mixed gas on the nitrogen reflected distributions. Two mixtures were used ($N_2$ with 9.15-percent Ar by mass and $N_2$ with 14.5-percent Ar by mass) and in-plane spatial distributions were determined for each species after steady-state reflected distributions developed. Results are shown in Figs. 24 and 25 (rectangular plot) and Figs. 26 and 27 (polar plot). Reference distributions necessary for estimation of capture coefficient were not obtained.

It is clear from the results that there is no significant effect of the argon on the nitrogen distributions, as shown by comparison with data for pure $N_2$. There is a slight shift of the lobe away from the surface, however.

A very noticeable seeding effect in the incident beam was observed for the argon. Because of acceleration by the lighter and more energetic $N_2$ molecules, the argon energies were significantly higher than would be obtained with pure argon from the same source temperature. The equivalent stagnation temperature for the argon was approximately 3500°K, as measured with the velocity distribution technique. The reflected distribution for the argon was much narrower than occurred for a 1670°K argon beam. Since higher temperatures have been observed to broaden the distribution for both argon (Ref. 11) and nitrogen, the narrow distribution may be attributed to gas interaction. It should be pointed out, however, that no experimental data for pure argon are available at the observed stagnation temperature of 3500°K.

## SECTION VIII
## CONCLUSIONS

An experimental investigation of a high temperature nitrogen beam impinging on a condensing surface of its own solid phase has been carried out. Steady-state reflected distributions and capture coefficient resulted after a period of frost buildup. The observed steady-state results may be summarized as follows:

1. The spatial distributions of reflected flux are highly lobular, with the maximum flux approximately 15 deg from the surface.

2. The dependence of lobe shape and location on incident beam temperature and angle of incidence is very small.

3. The capture coefficient decreases with increasing incident gas stagnation temperature.

4. The capture coefficient decreases with increasing angle of incidence from normal.

5. The observed trends are nearly identical to those reported for argon (Ref. 11) and predicted by a hard sphere model (Ref. 12).

An additional experiment with nitrogen-argon mixtures revealed no significant differences from single species behavior, except for the seeding effect in the incident beam which accelerates the heavier gas.

Transient effects investigated revealed a gradual buildup of the reflected distribution from a condensing surface with no previous cryodeposit, accompanied by a decrease in capture coefficient from near unity to the steady-state value. Interruption of the beam after attainment of steady state produced initially higher capture coefficients on resumption, indicating changes in the frost layer during interruption.

These results for nitrogen and for argon provide new and potentially useful information on the basic gas-cryosurface interactions. From the transient data, it is probable that for many short-duration rocket plume tests, cryosystem performance will be better than steady-state predictions. Capture coefficients for gases in directed flow are also maximized for near-normal incidence.

## REFERENCES


1. Wang, E. S. J., Collins, J. A., Jr. and Haygood, J. D. "General Cryopumping Study." Advances in Cryogenic Engineering. Vol. 7, K. D. Timmerhaus (ed.), Plenum Press, Inc., New York, 1962.

2. Dawson, J. P. "Cryopumping Capture Coefficients of Two Nitrogen-Oxygen Gas Mixtures." AEDC-TDR-64-150 (AD603623), August 1964.

3. Moody, T. L. "Capture Coefficient of 300°K $CO_2$ on a 77°K Surface as Measured by the Rotating Gage Technique." AEDC-TR-66-231 (AD645510), January 1967.

4. Stickney, R. E. "Atomic and Molecular Scattering from Solid Surfaces." Advances in Atomic and Molecular Physics (D. R. Bates and I. Esterman) editors, 3, Academic Press, New York, 1967, p. 186.

5. Brown, R. F. and Heald, J. H., Jr. "Description and Performance of a Molecular Beam Chamber Used for Cryopumping and Adsorption Pumping Studies." AEDC-TR-66-135 (AD641388), October 1968.

6. Heald, J. H., Jr. "Performance of a Mass Spectrometric Modulated Beam Detector for Gas-Surface Interaction Measurements." AEDC-TR-67-35 (AD648984), March 1967.

7. Powell, H. M. and Heald, J. H., Jr. "A System for the Measurement of Velocity Distributions of Molecular Beams." AEDC-TR-68-151 (AD675306), September 1968.

8. Benek, J. A., Busby, M. R. and Powell, H. M. "A Technique for the Analysis and Computerized Data Reduction of Velocity Distributions of Free Jet Expansions." AEDC-TR-70-84, October 1970.

9. Heald, J. H., Jr. and Brown, R. F. "Measurements of Condensation and Evaporation of Carbon Dioxide, Nitrogen, and Argon at Cryogenic Temperatures Using a Molecular Beam." AEDC-TR-68-110 (AD674596), September 1968.

10. Caldwell, R. L., Busby, M. R. and Brown, R. F. "Spatial Distributions of 285°K to 2500°K Argon Beams Scattered from an Undefined Copper Surface at Temperatures between 36°K and 285°K." AEDC-TR-69-142 (AD698325), December 1969.

11. Busby, M. R. and Brown, R. F. "An Experimental Investigation of the Scattering of a Monoenergetic Argon Molecular Beam from a Solid Argon Surface." AEDC-TR-70-90, October 1970.

12. Busby, M. R., Haygood, J. D. and Link, C. H. "A Classical Model for Gas-Surface Interaction." AEDC-TR-70-131, July 1970.

13. Ruby, Earl C., Jr. "An Experimental Study of the Velocity Distribution and Relative Abundances of Argon Molecular Clusters in the Condensation Region of a Free Jet." M. S. Thesis, University of Tennessee, December 1969.

14. Trischka, J. W. Methods of Experimental Physics 3: Molecular Physics, Ed. by D. Williams, Academic Press, New York, New York, 1962.

15. Fite, W. L. and Brackmann, R. T. "Collisions of Electrons with Hydrogen Atoms. I. Ionization." Phys. Rev., Vol. 112, 1141 (1958).

16. Fite, W. L. and Datz, S. "Chemical Research with Molecular Beams." Annual Review of Physical Chemistry. Annual Reviews, Inc., Stanford, California, Vol. 14, 1963, pp. 61-68.

17. Anderson, J. B., Andres, R. R. and Fenn, J. B. "Supersonic Nozzle Beams." Advances in Chemical Physics, J. Ross, ed., Vol. 10, New York, John Wiley and Sons, Inc., 1966, pp. 275-318.

# APPENDIX

# ILLUSTRATIONS

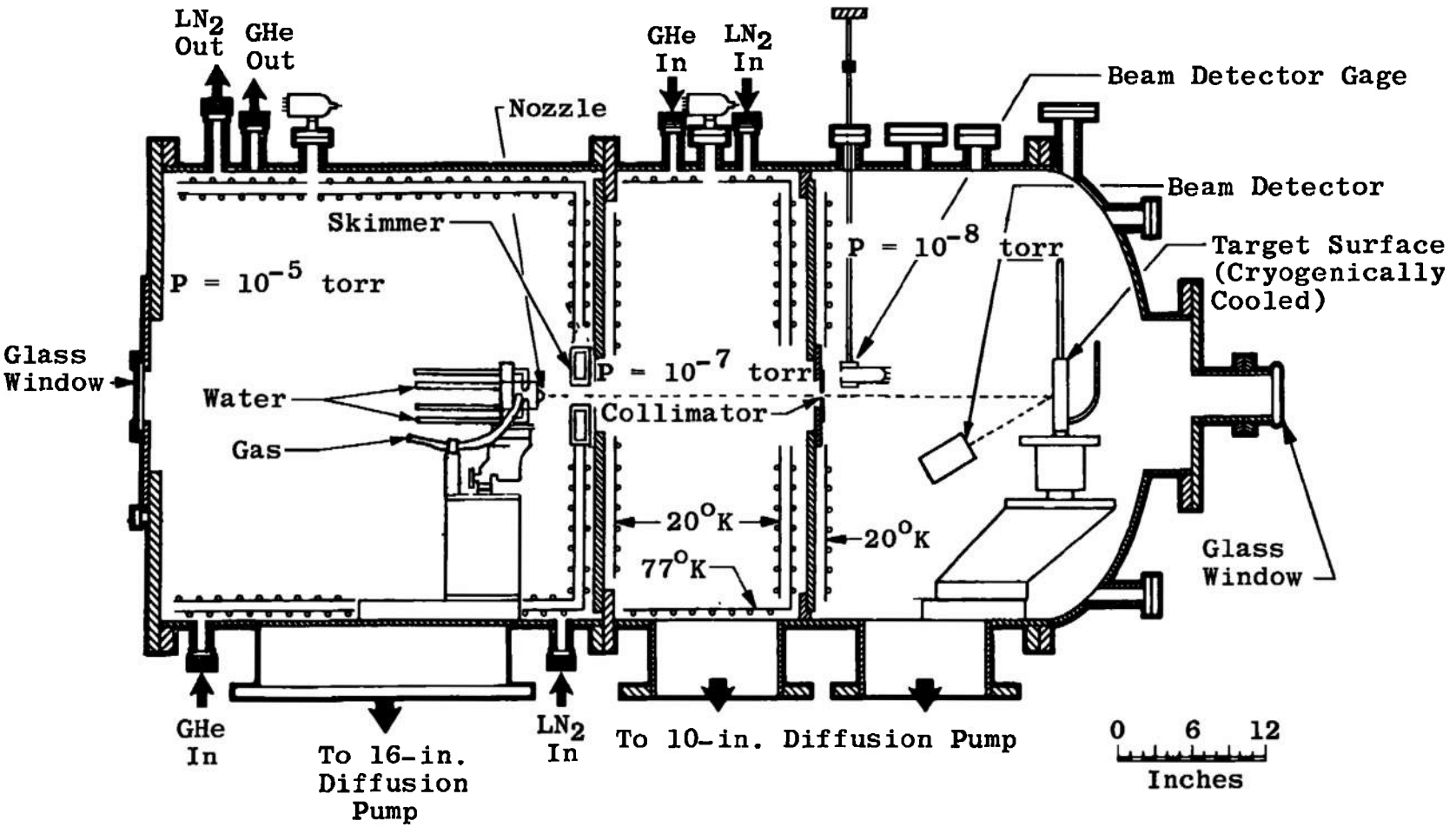


Fig. 1 Aerodynamic Molecular Beam Chamber



AEDC-TR-70-172

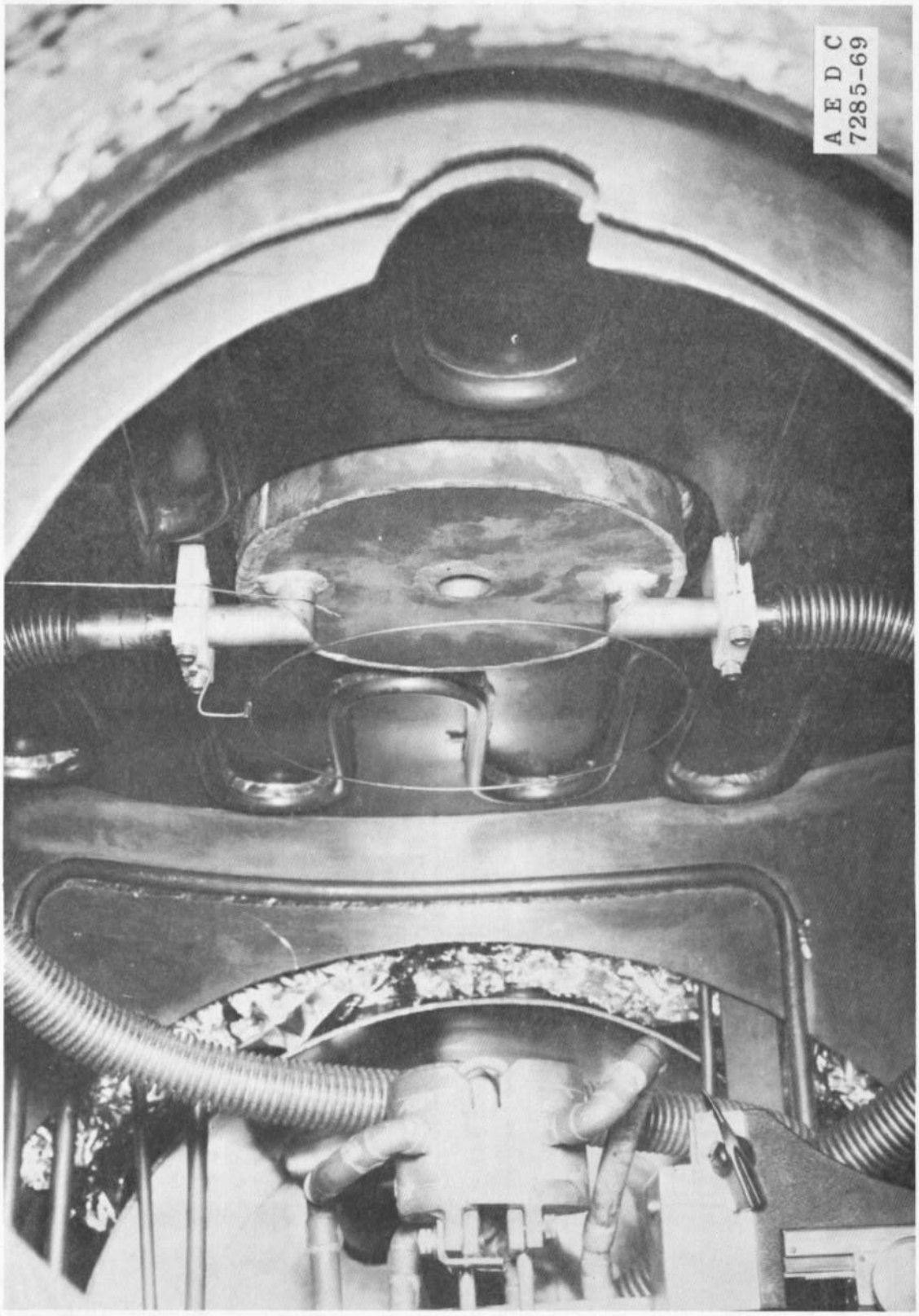


Fig. 2 Photograph of the Gas Source and Cryogenically Cooled Skimmer

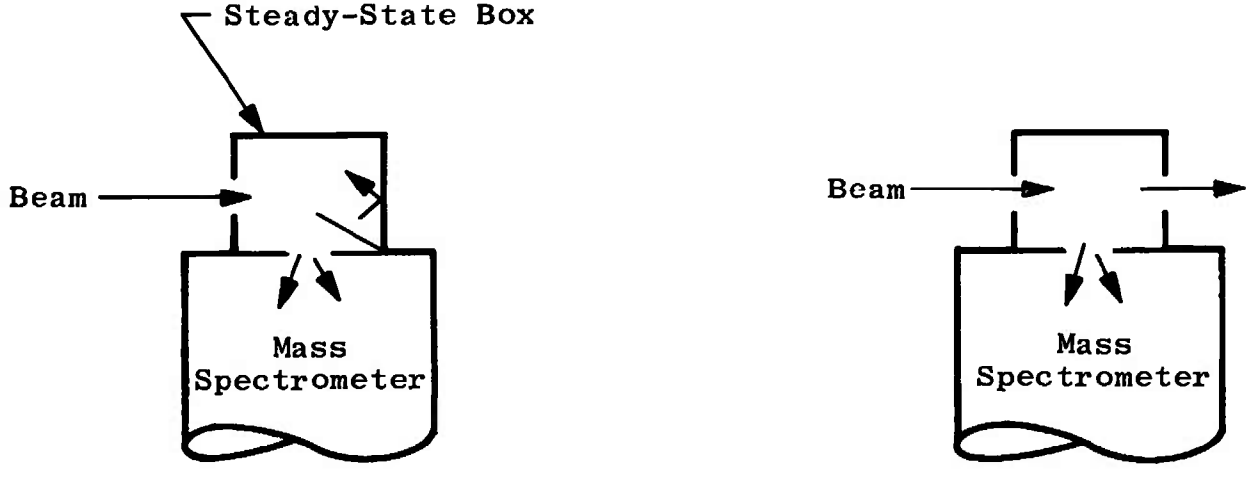


a. Molecular Flow Rate Detector

b. Molecular Flow Density Detector

Fig. 3 Operational Modes of the Detector

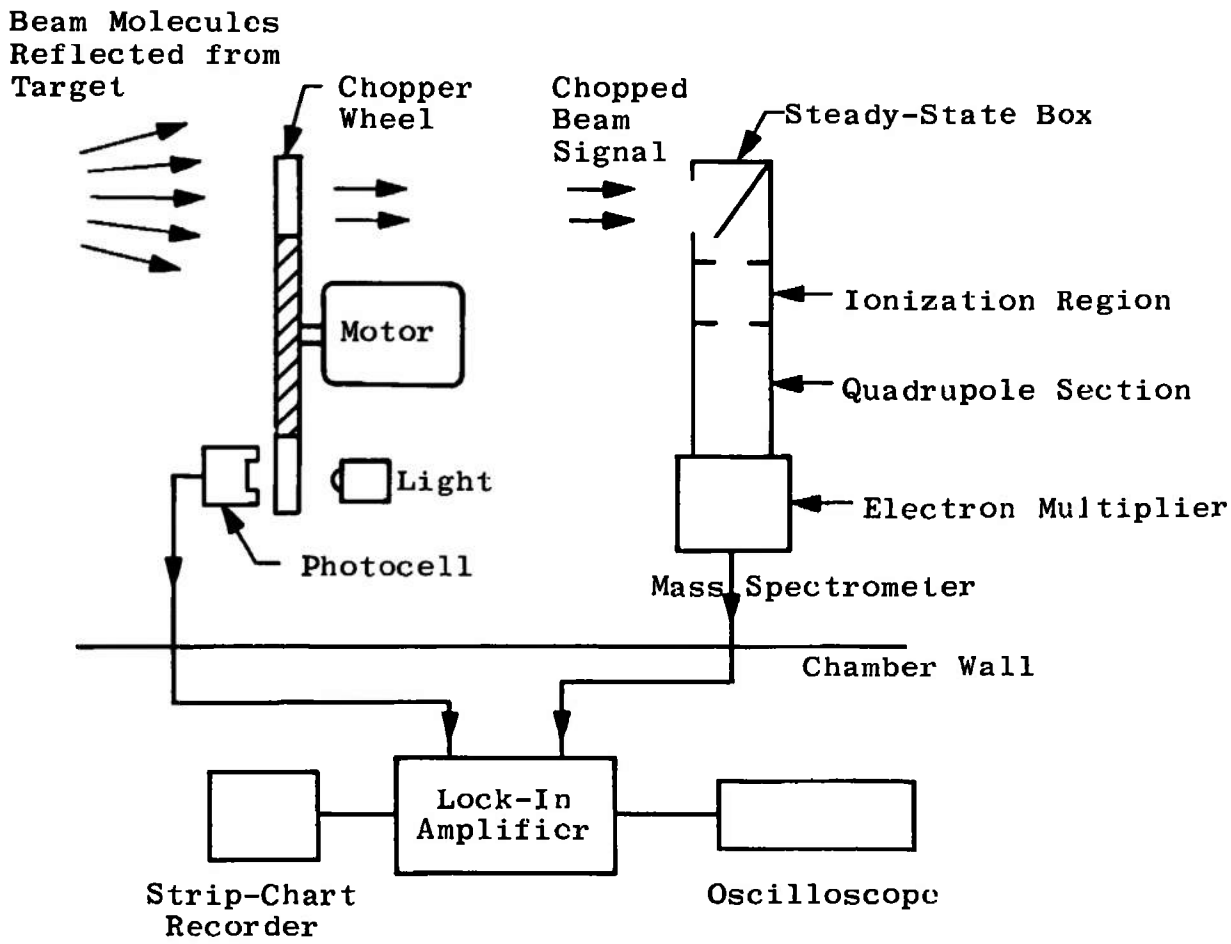


**Fig. 4 Schematic of Mass-Spectrometric Modulated Beam Detector**

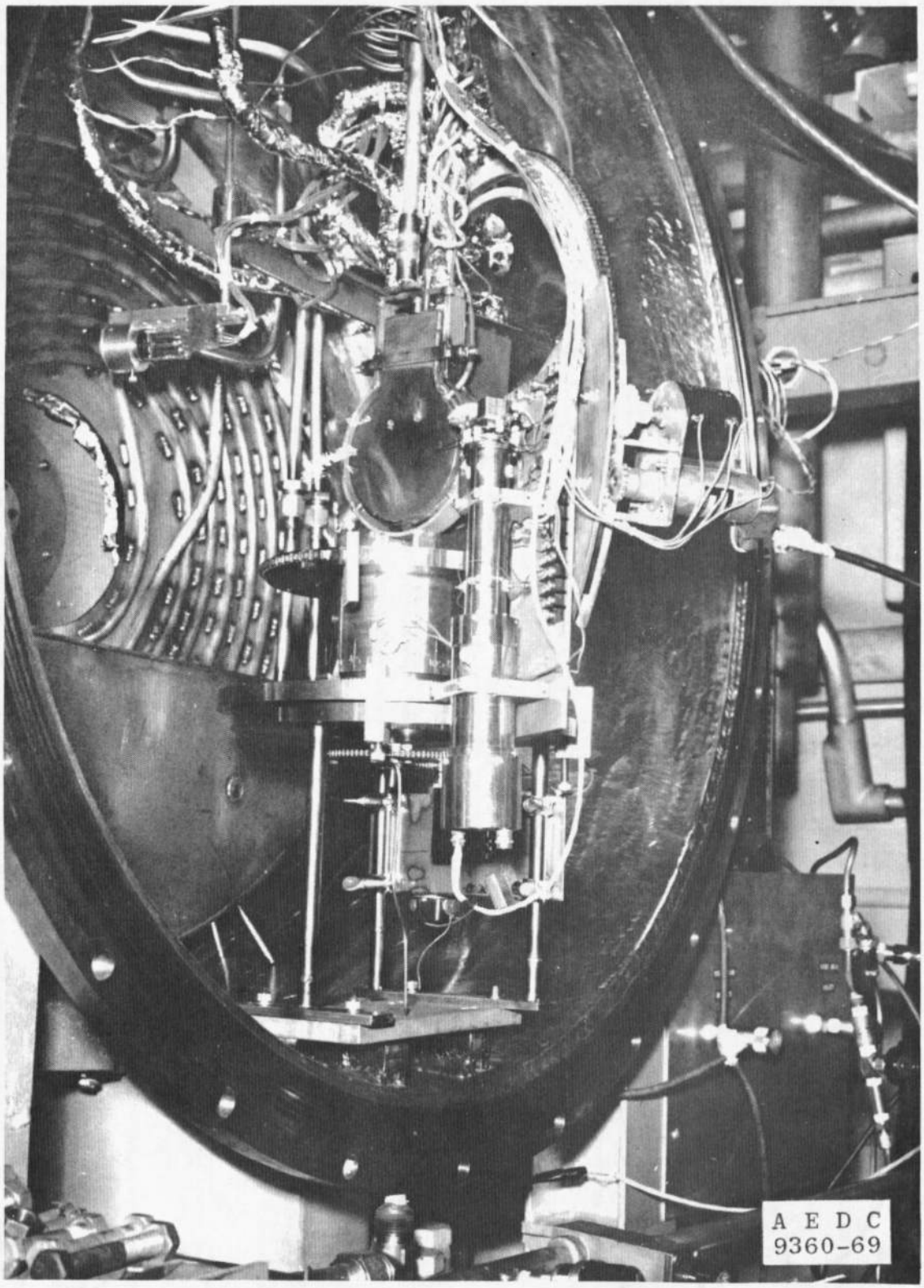


Fig. 5 Photograph of the Target and Detector Movement Mechanisms

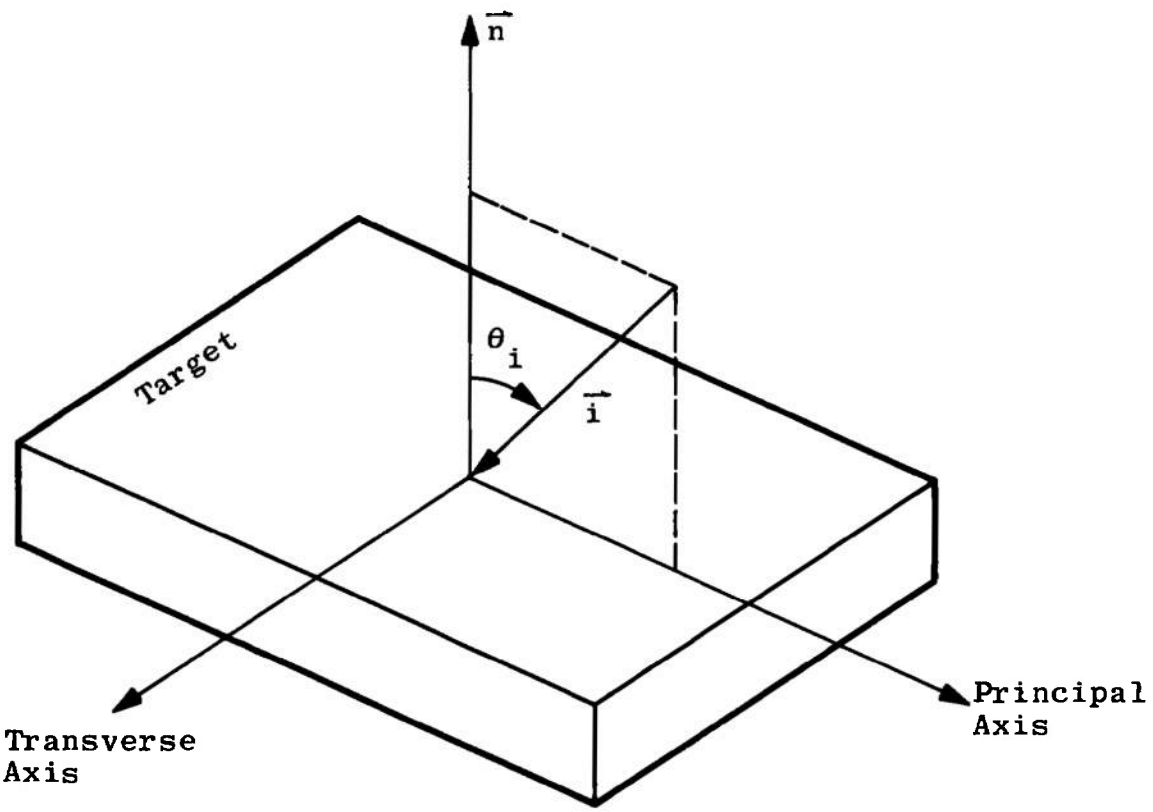


Fig. 6 Orientation Parameters for the Incident Beam

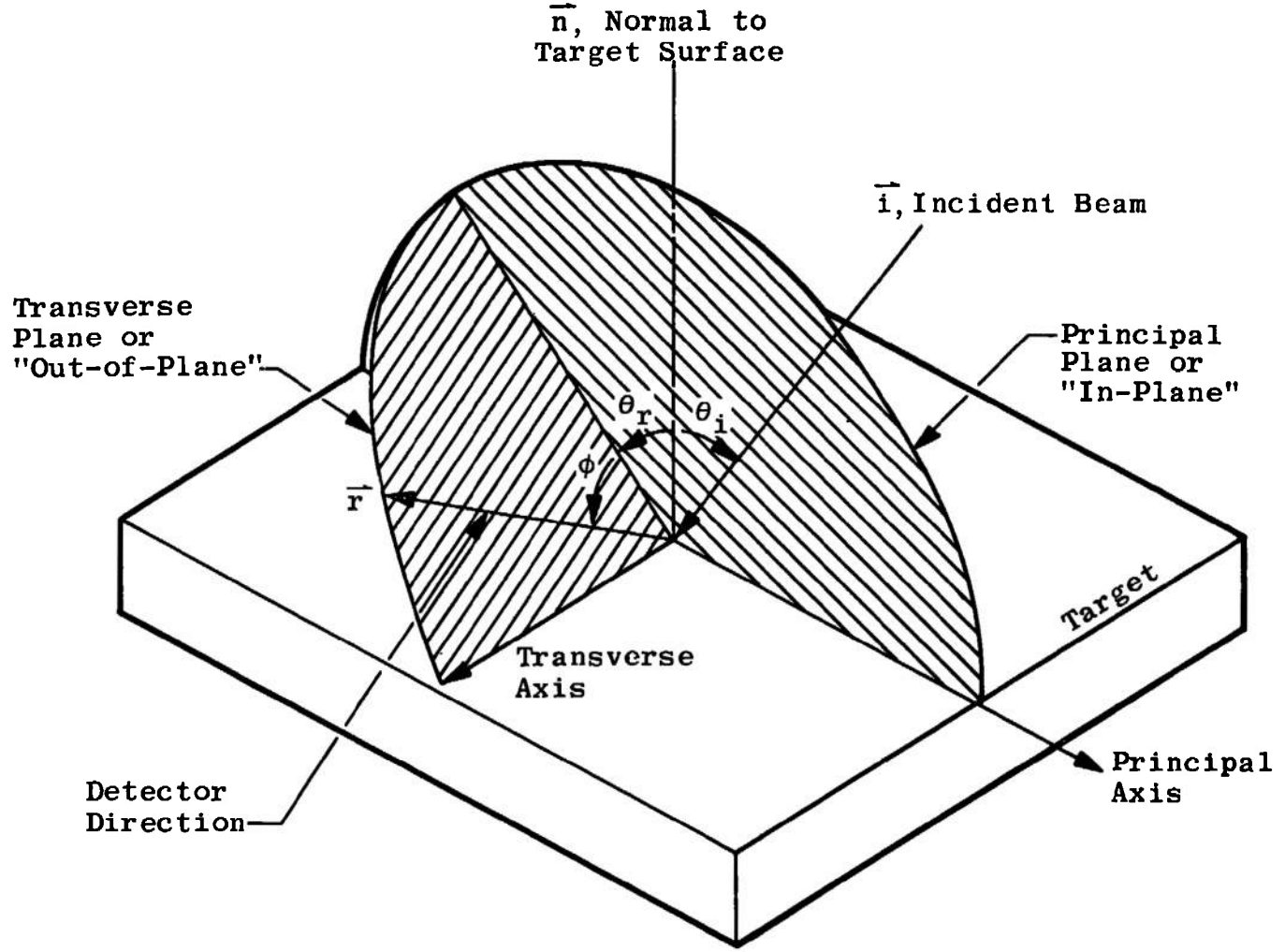


Fig. 7 Orientation Parameters for the Reflected Beam

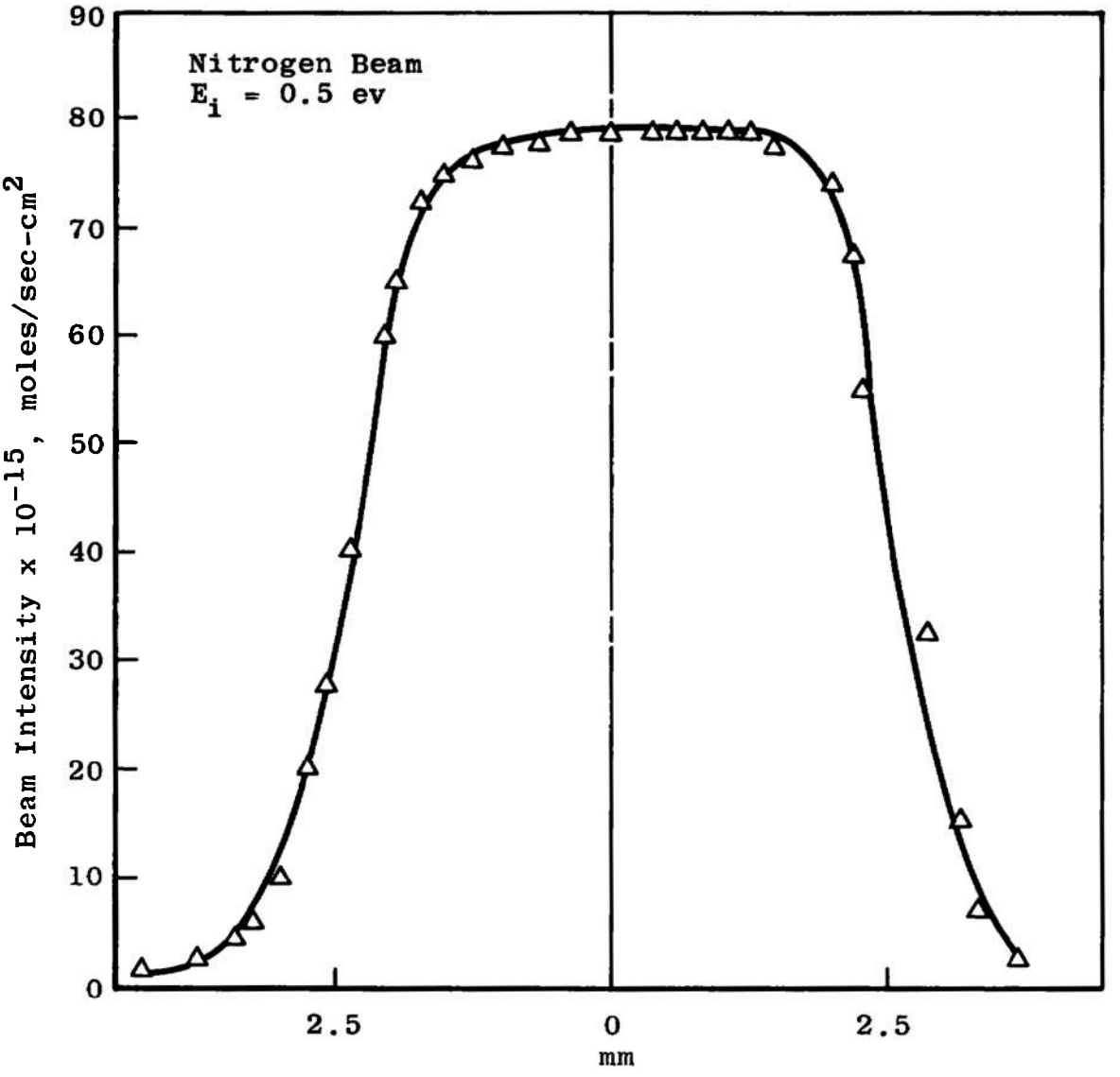


Fig. 8 Intensity Cross Section of the Beam

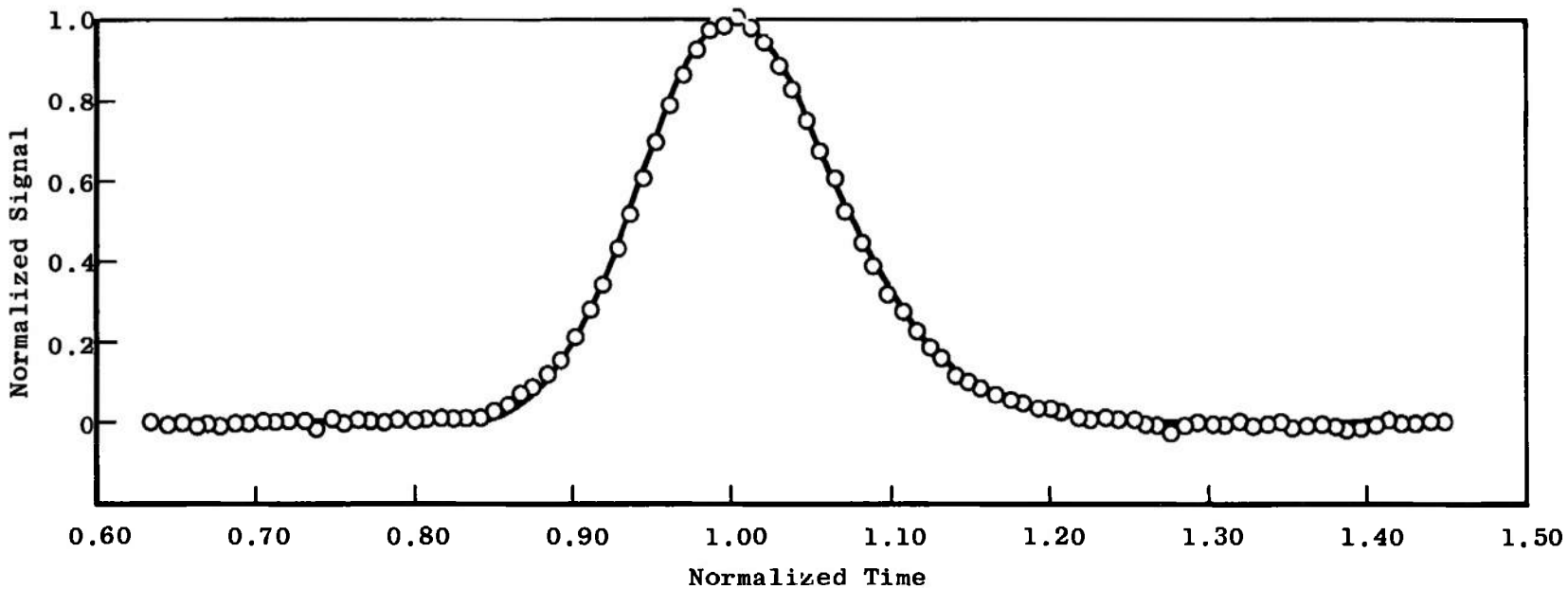


Fig. 9 Time-of-Flight Distribution of a 0.44-ev Nitrogen Beam

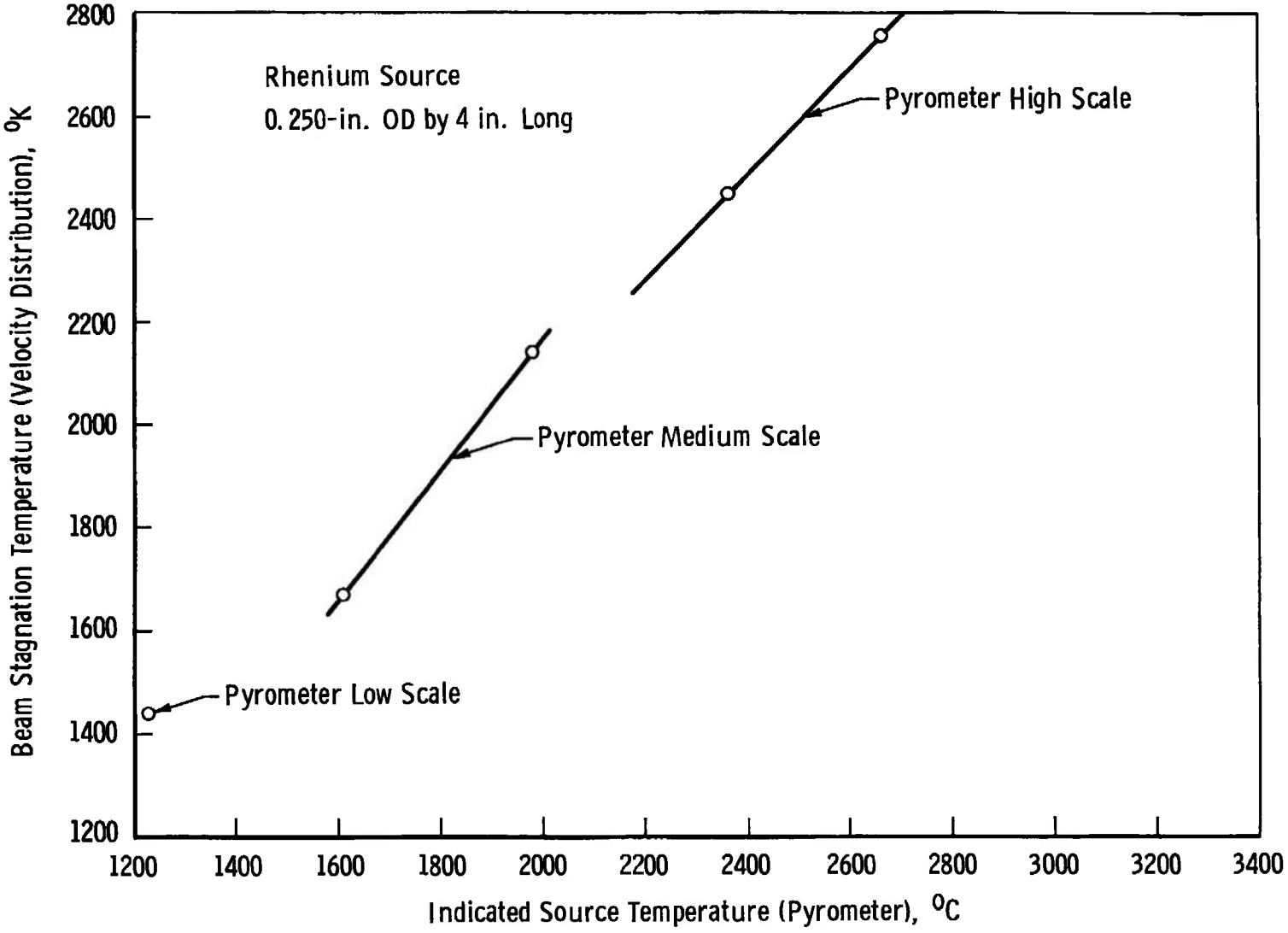


**Fig. 10 Beam Tempersture versus Indicated Source Temperature**

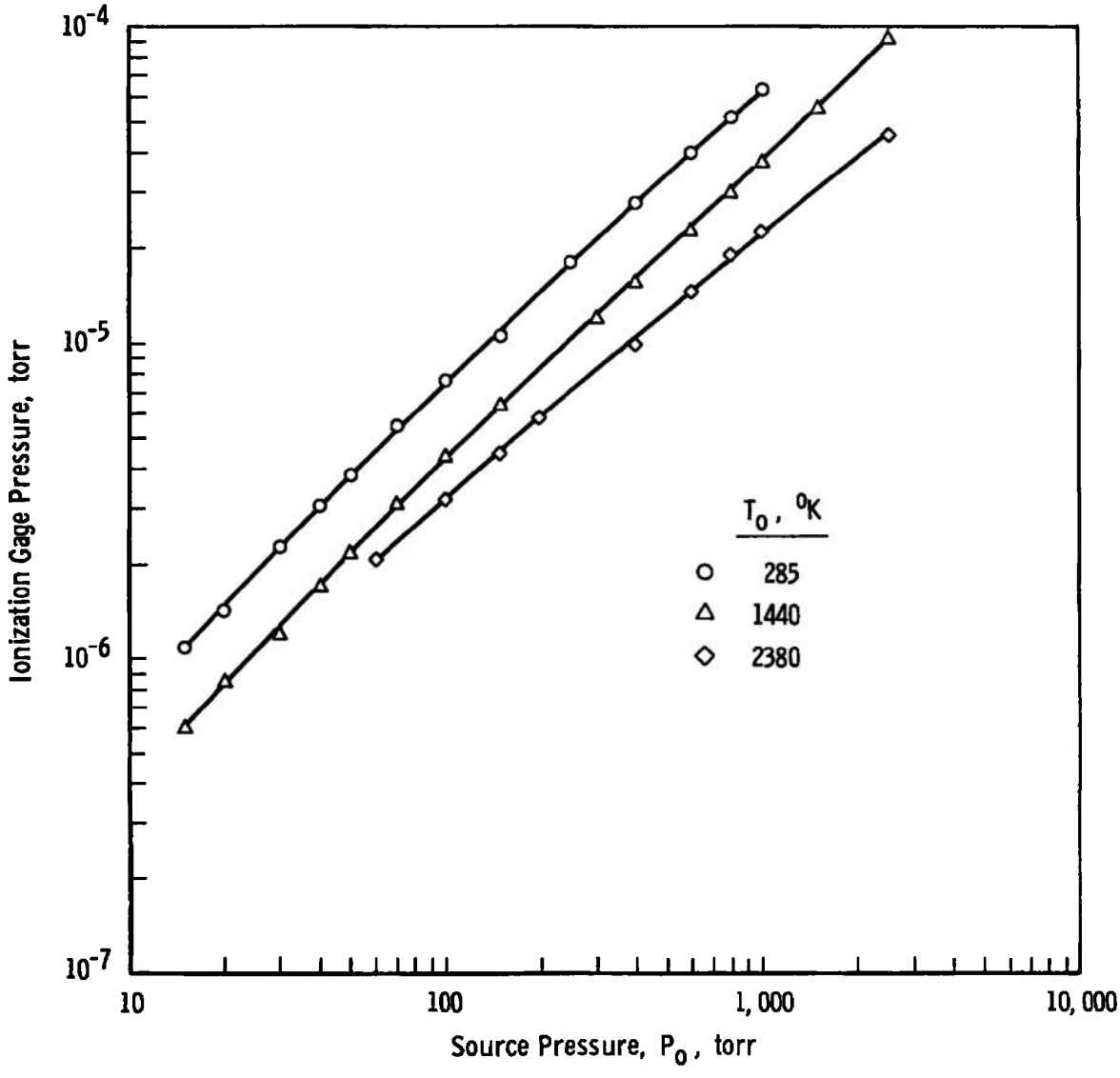


**Fig. 11 Nitrogen Beam Performance**

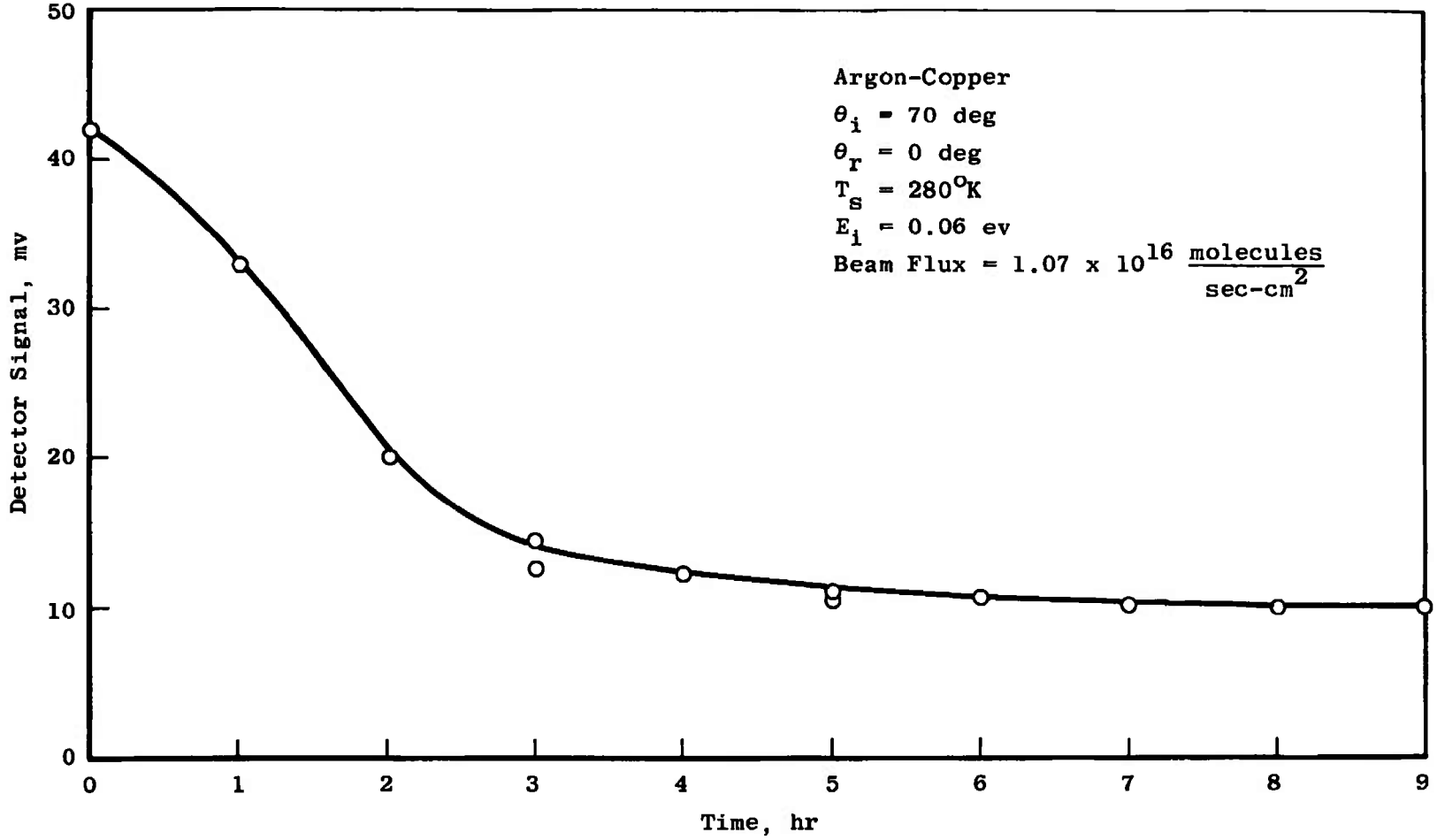


Fig. 12 Variation of Multiplier Sensitivity

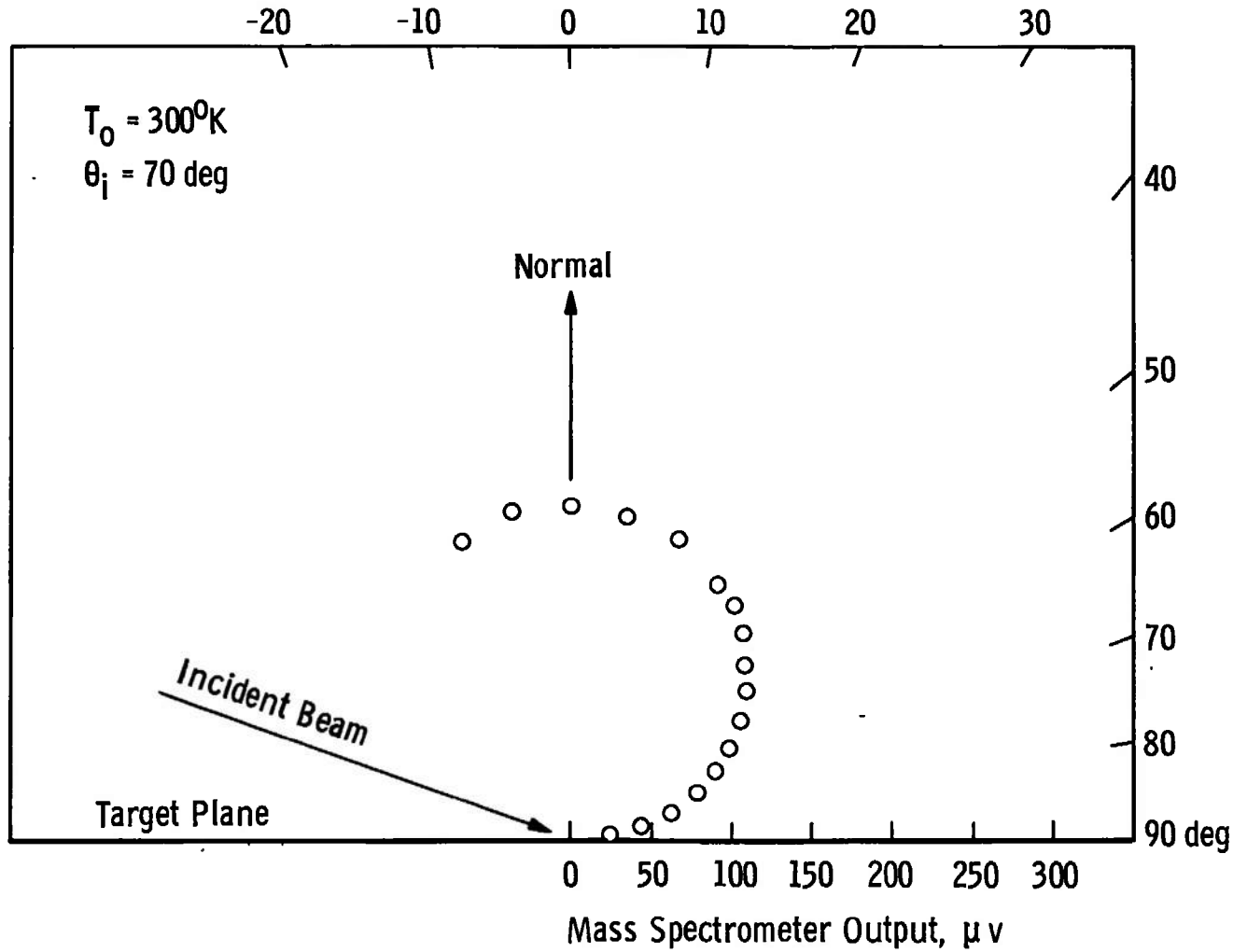


Fig. 13 Reflected Distribution for Incidence 70 deg from Normal and 36° K Target Temperature

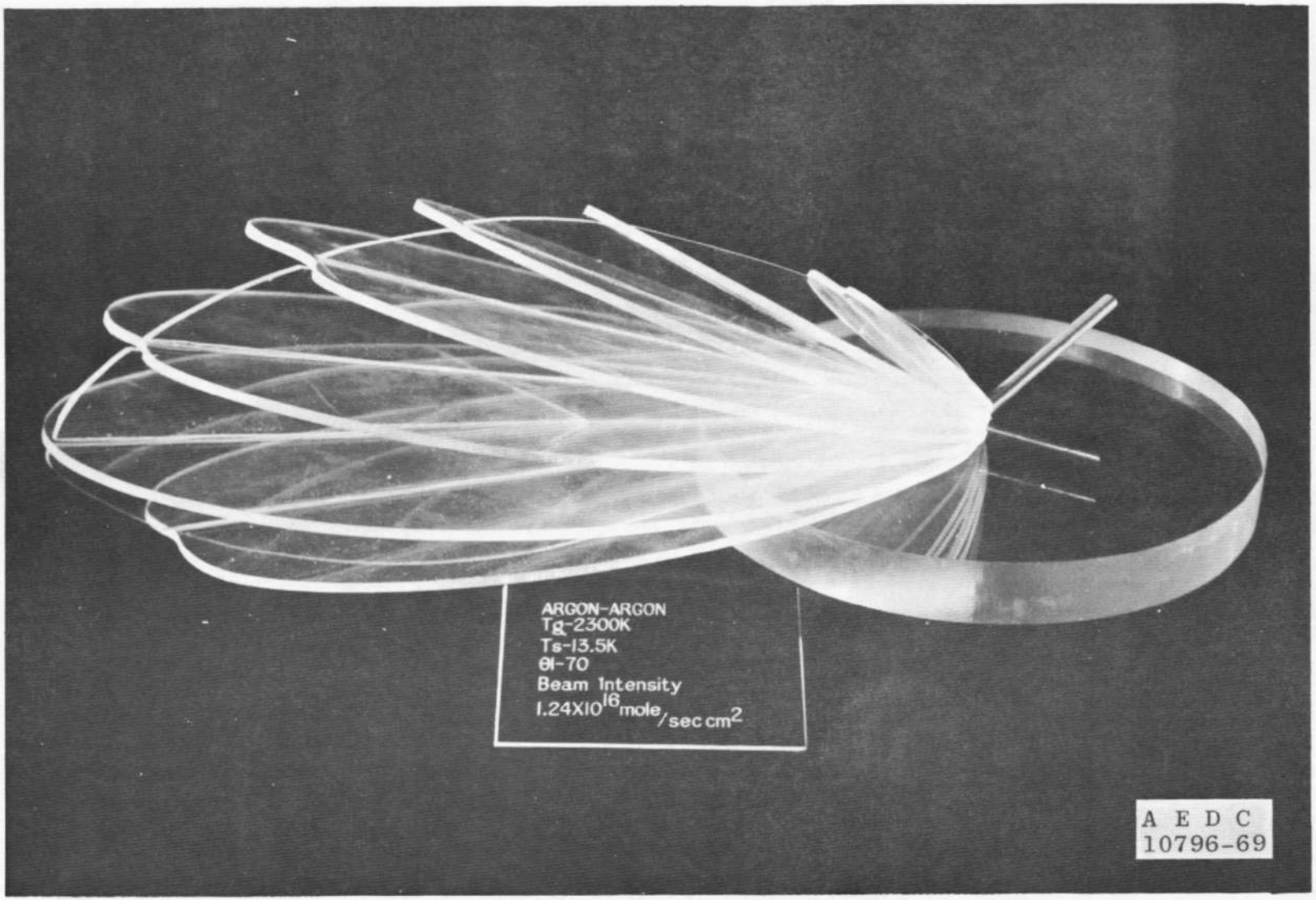


Fig. 14 Photograph of a Model of a Typical Scattering Distribution

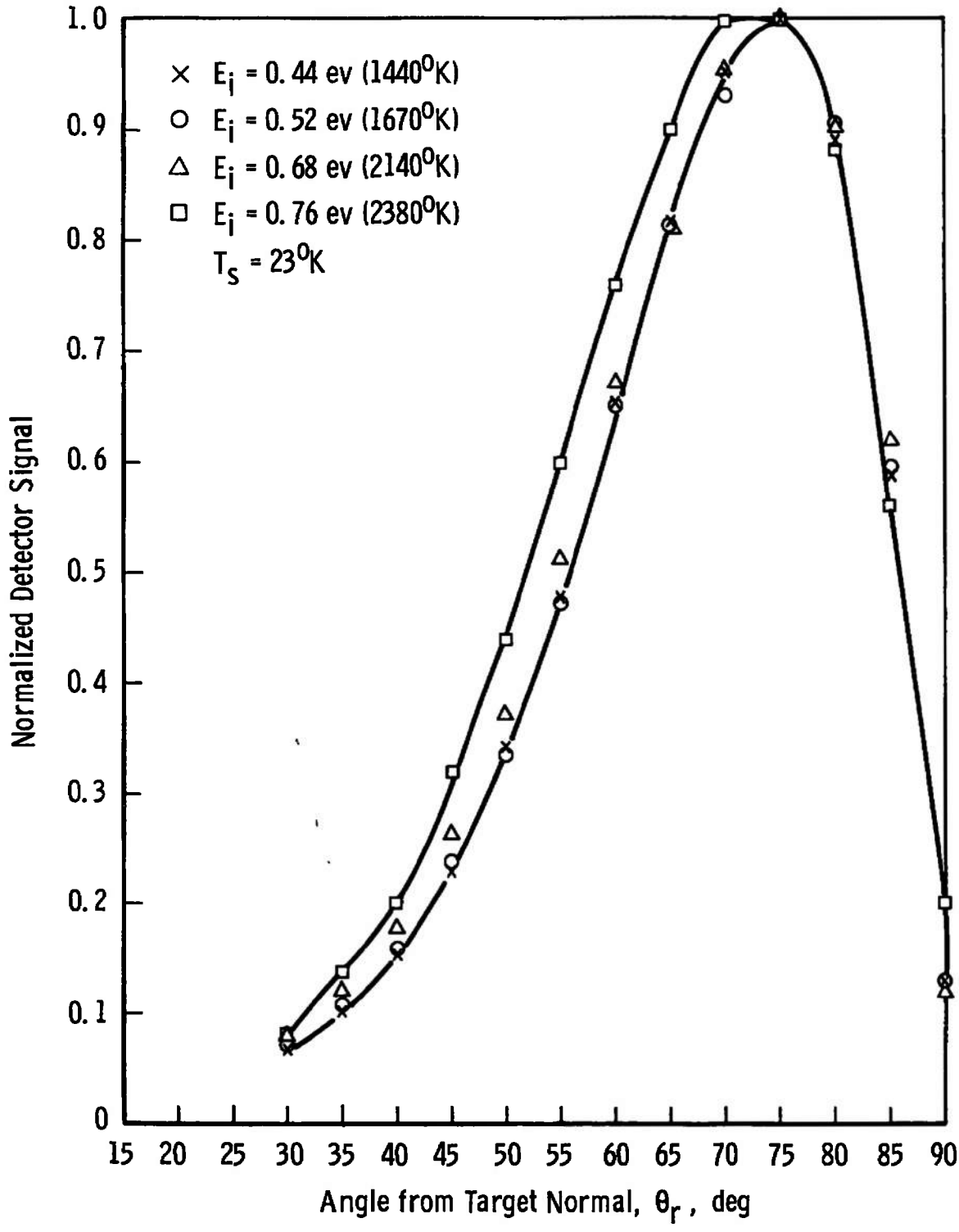


**Fig. 15 Reflected In-Plane Distribution for Incidence 70 deg from Normal and 23° K Target Temperature**

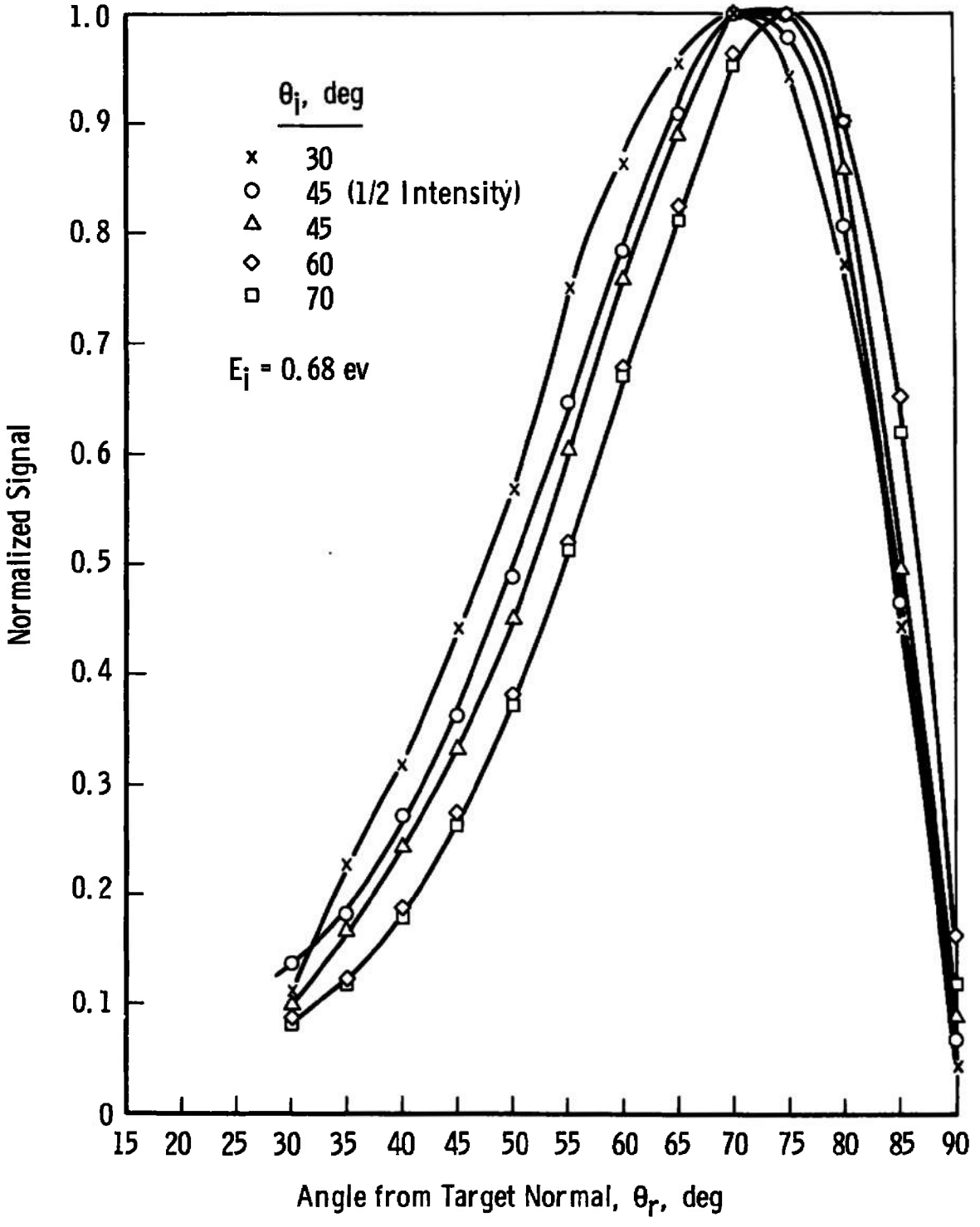


**Fig. 16 Reflected In-Plane Distribution for 2000°K Incident Beam**

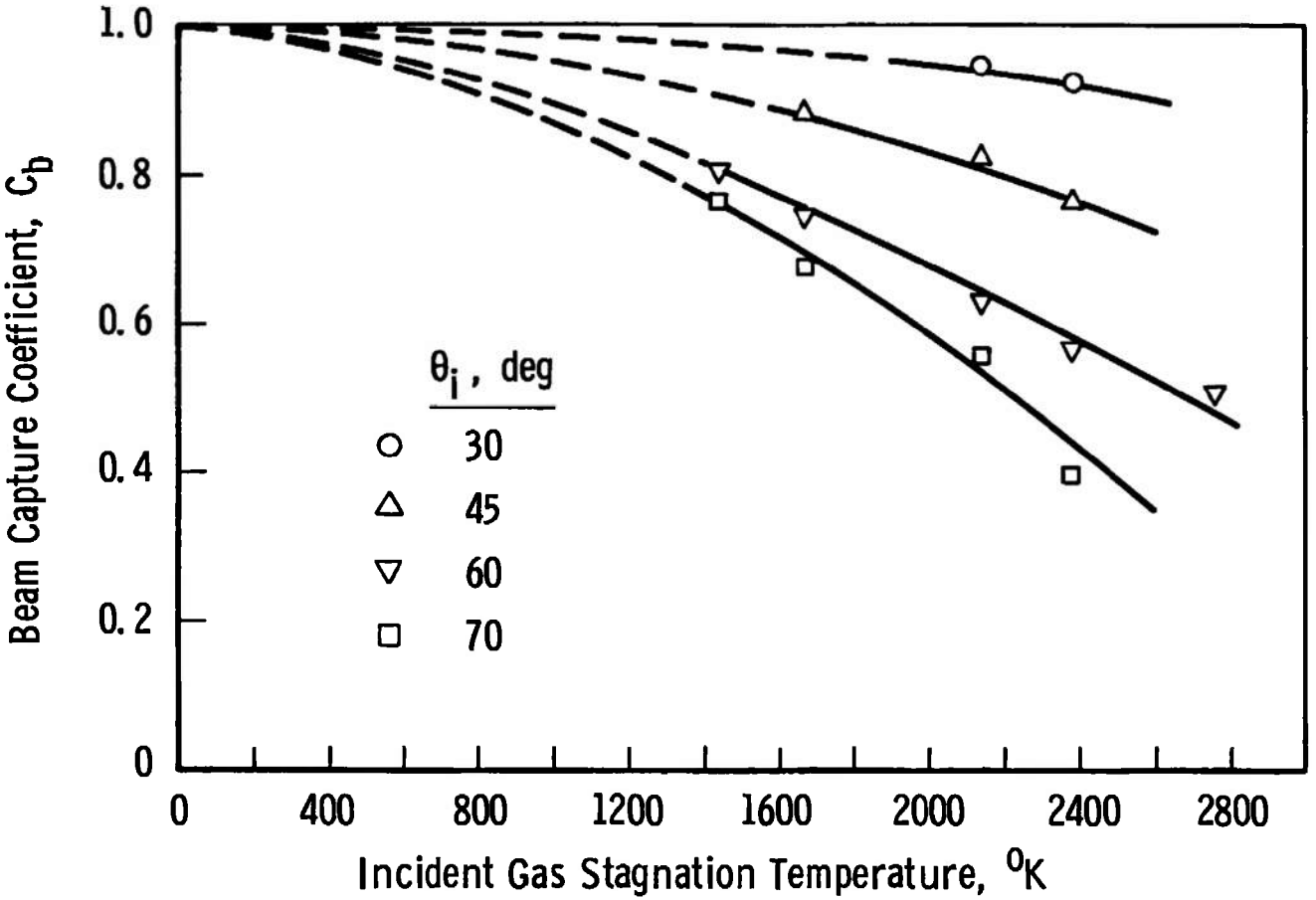


Fig. 17 Capture Coefficient versus Incident Gas Temperature

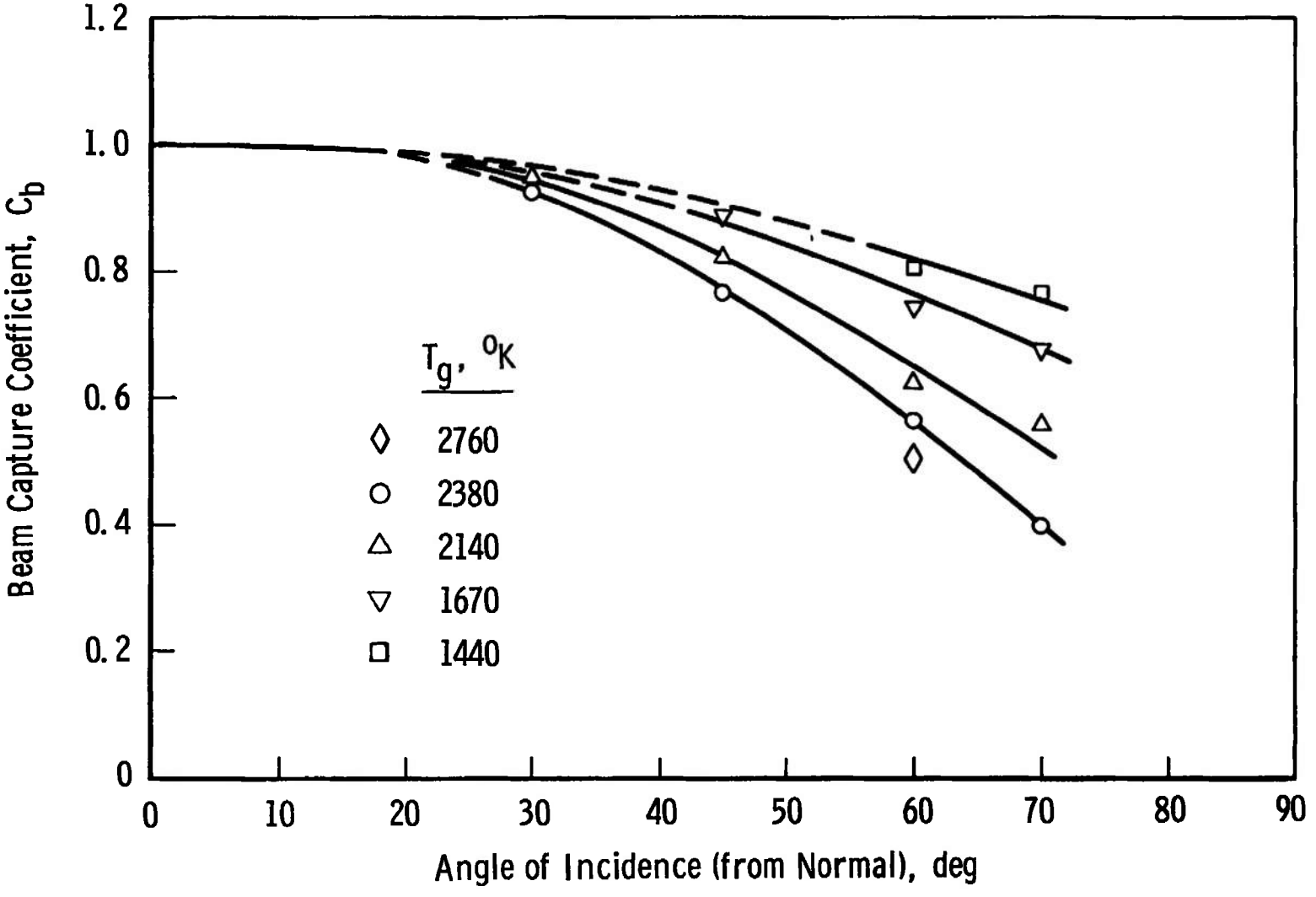


Fig. 18 Capture Coefficient versus Angle of Incidence from Normal

$$1 - C = \frac{\dot{n}_r}{\dot{n}_t} = \frac{\frac{2}{\pi} \int_0^{\frac{\pi}{2}} \int_0^{\frac{\pi}{2}} S(\theta, \phi) \cos\phi \, d\theta \, d\phi}{S_{ref}}$$

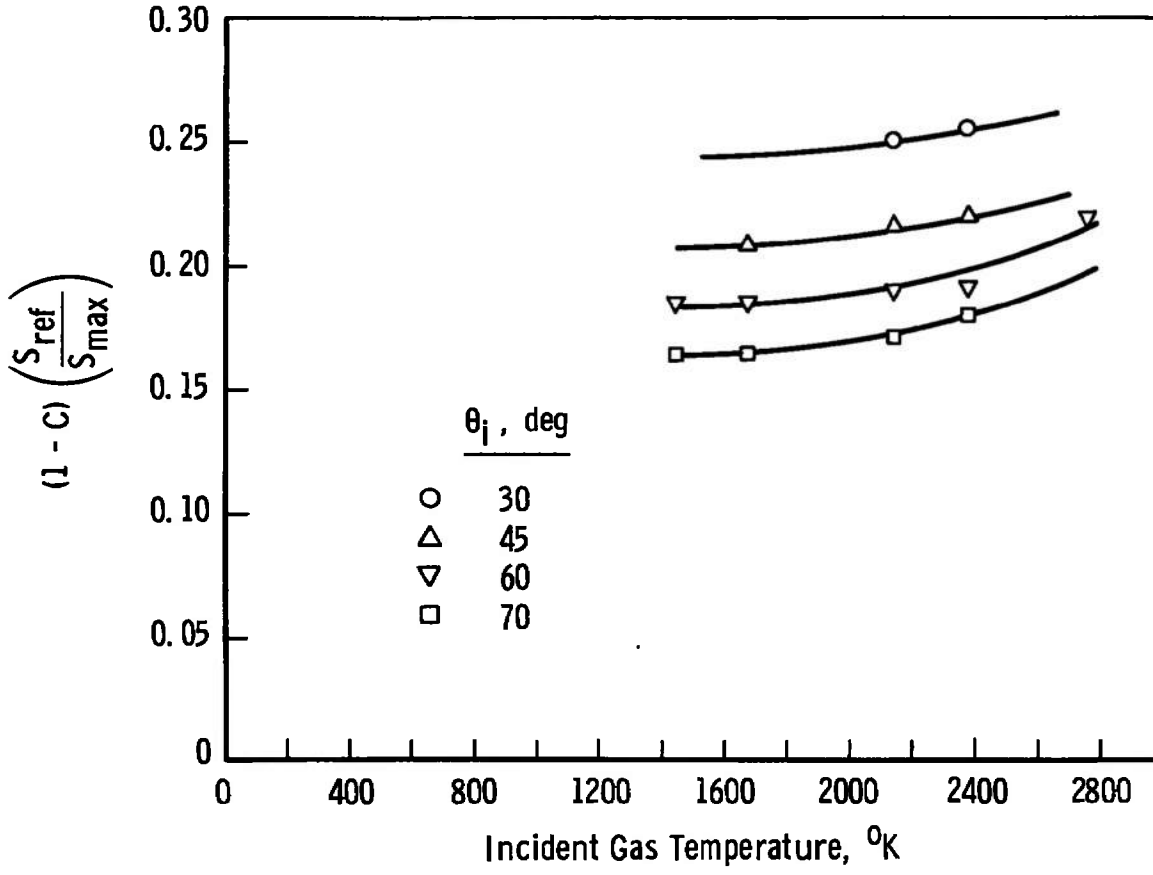


**Fig. 19 Normalized Reflected Flux Ratio versus Incident Gas Temperature**

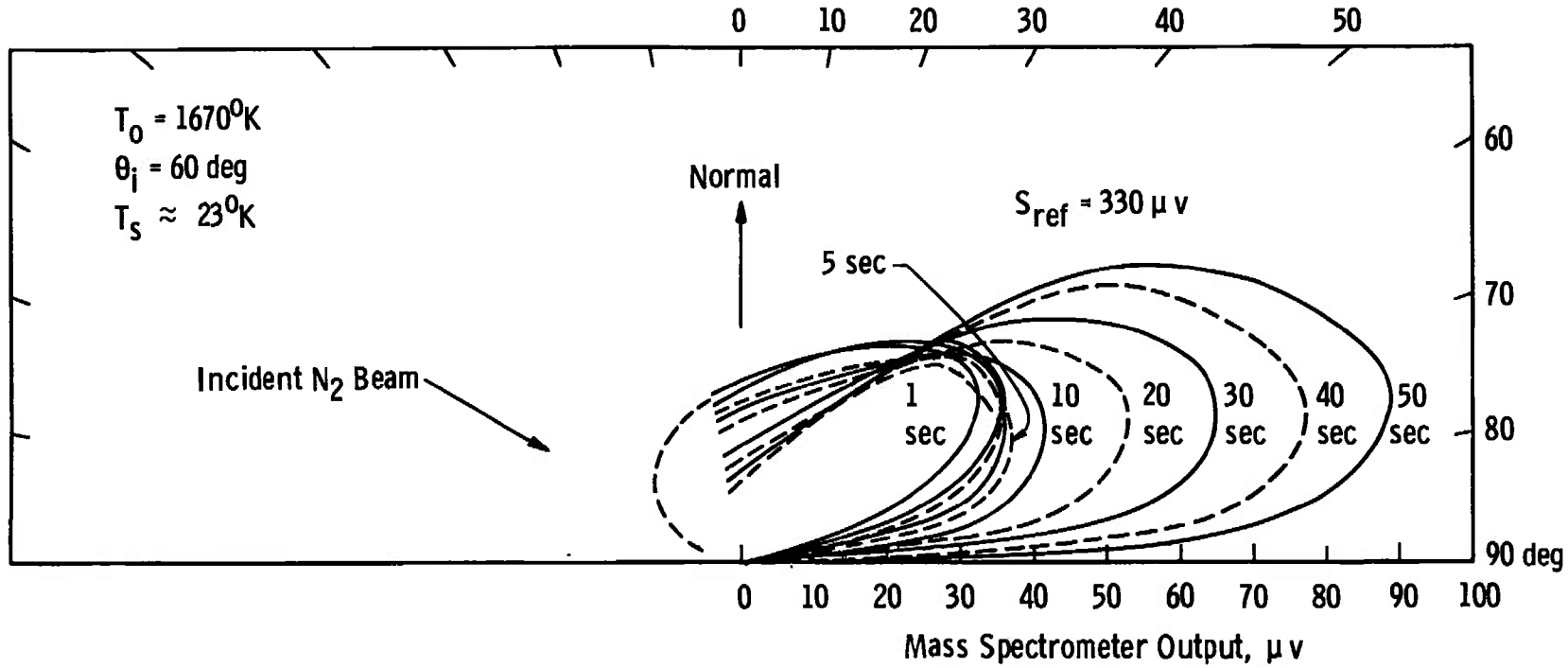


**Fig. 20 Initial Buildup of Reflected Flux (In-Plane) for Target with no Previous Cryodeposit**

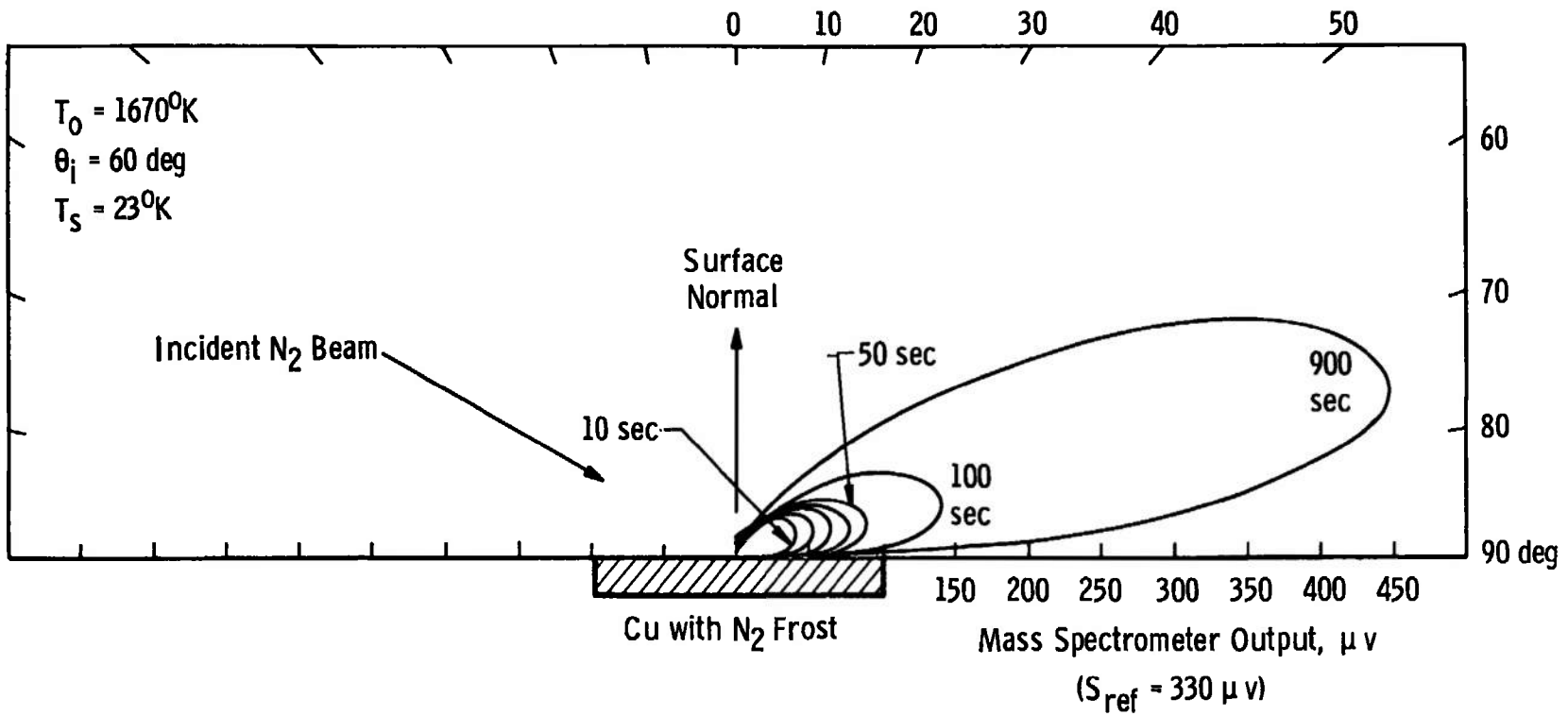


**Fig. 21 Buildup of Reflected Flux (In-Plane) for Target with no Previous Cryodeposit**

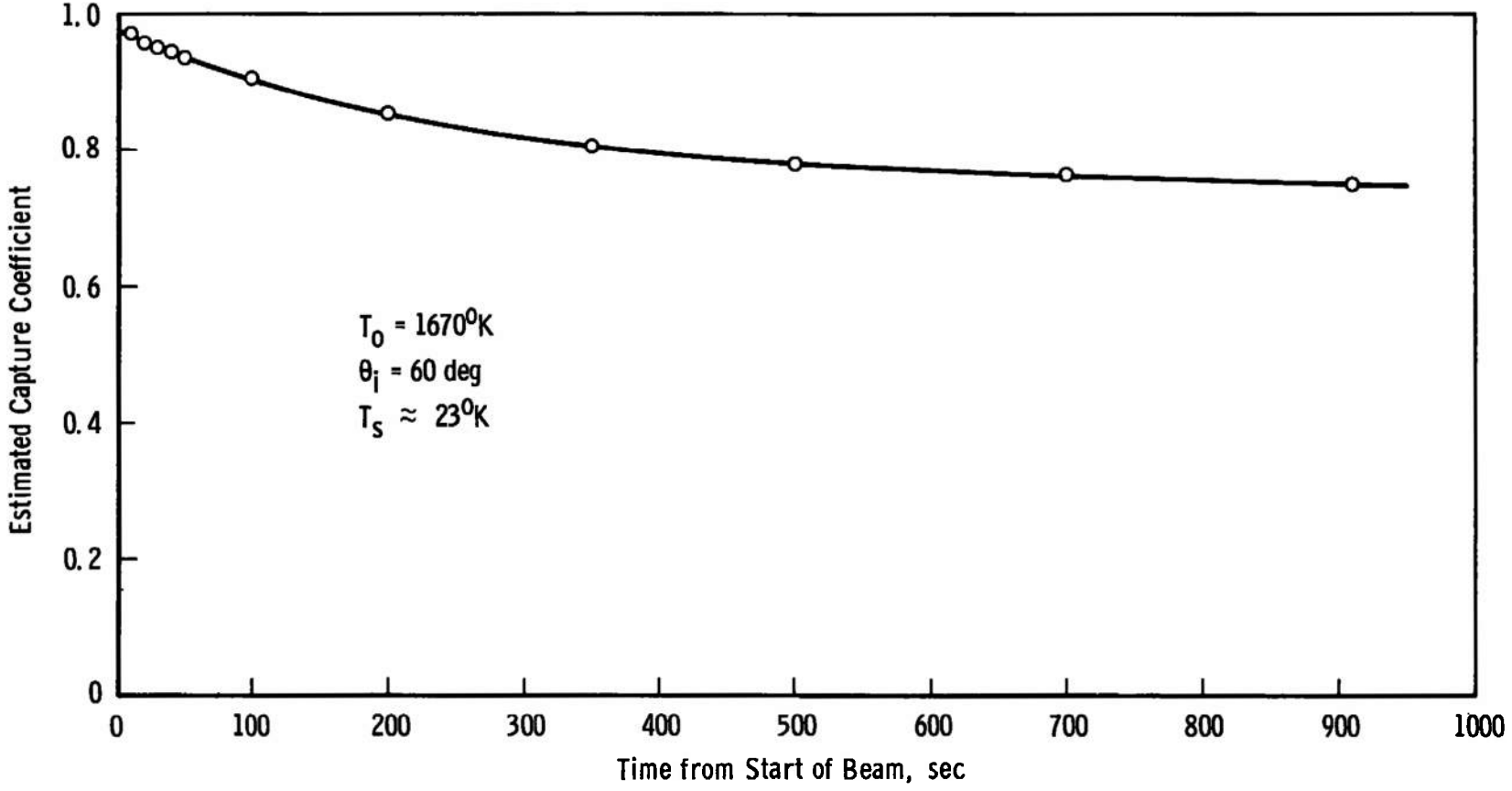


**Fig. 22 Estimated Capture Coefficient versus Time for Target with no Previous Cryodeposit**

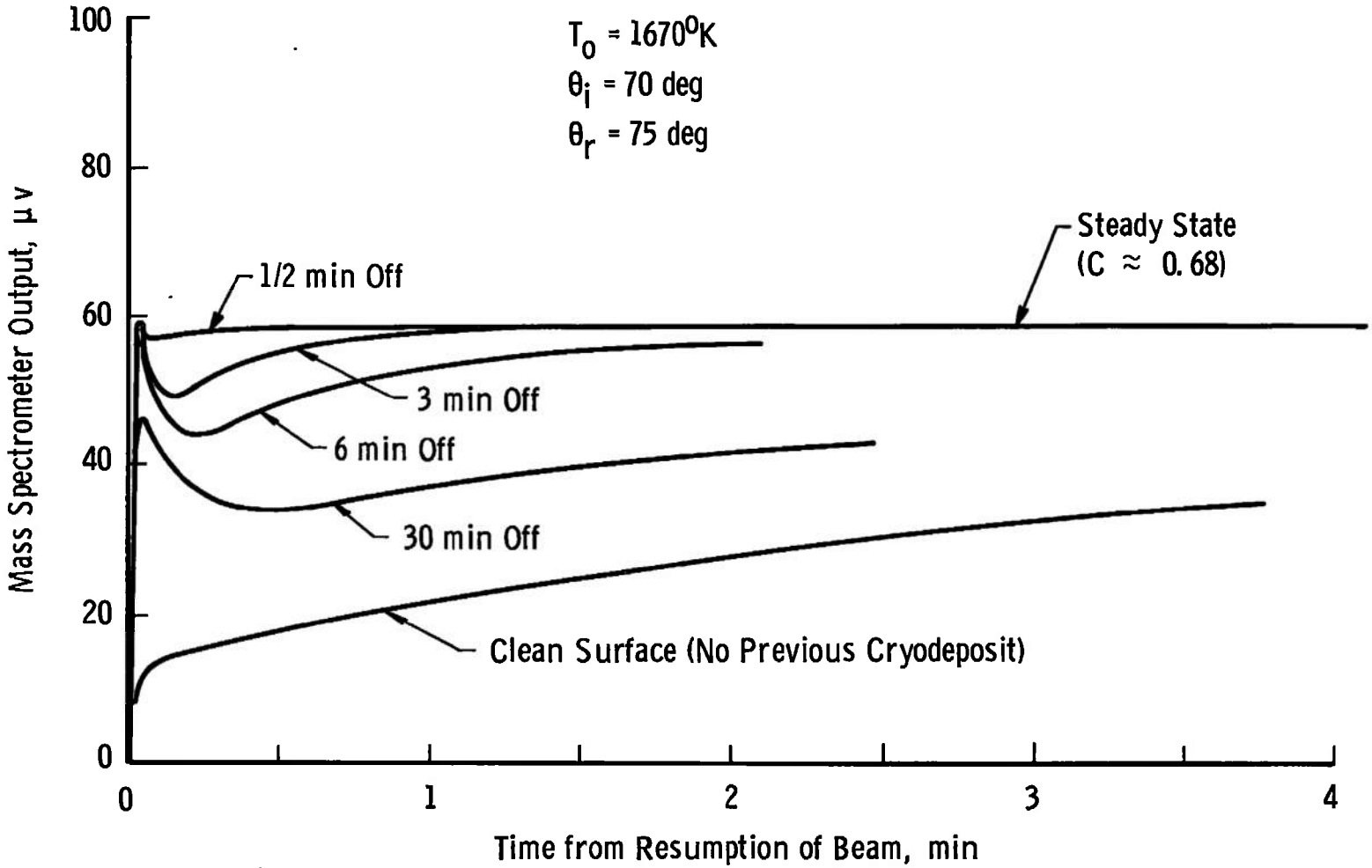


Fig. 23 Effect of Beam Interruption on Reflected Flux Intensity

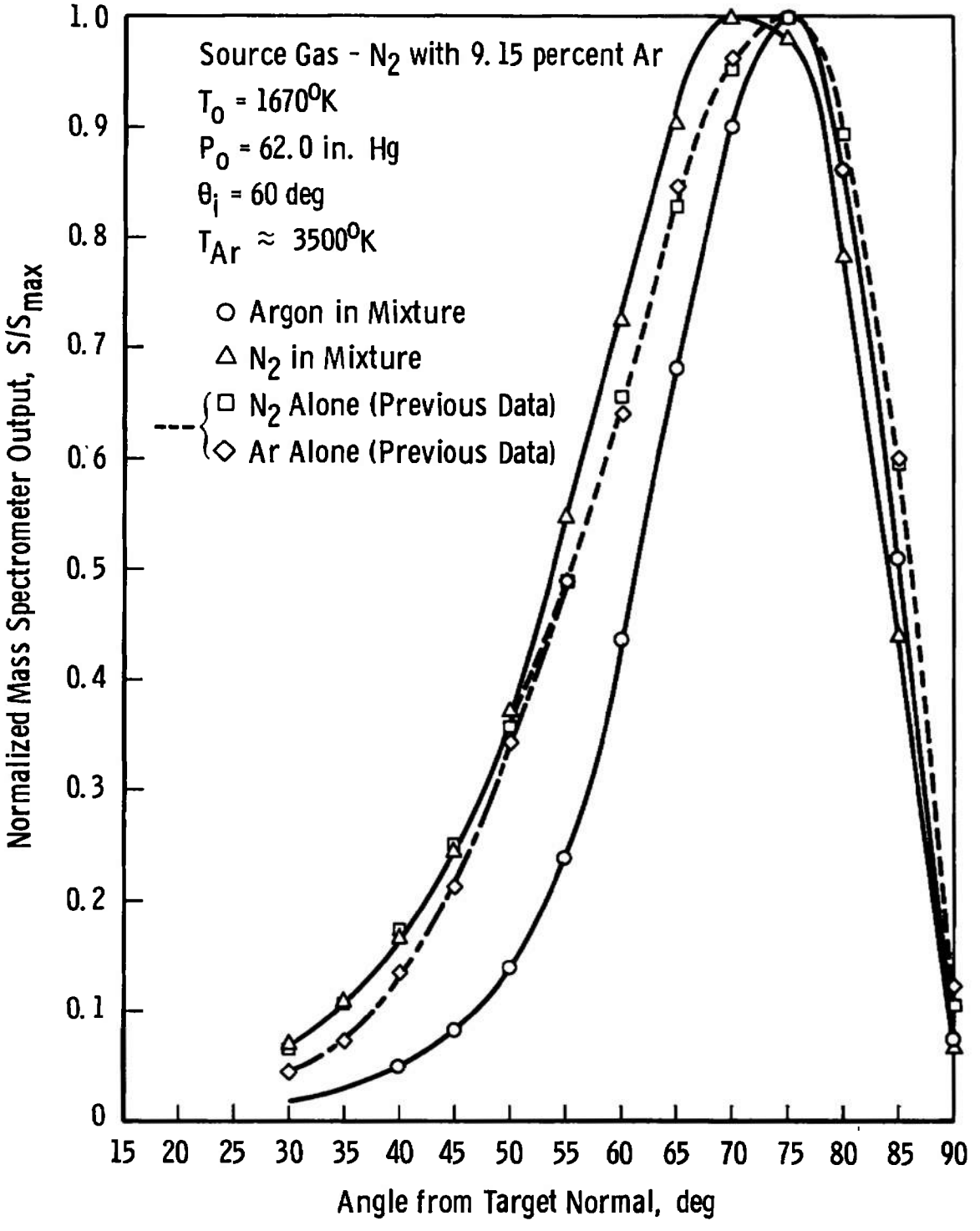


**Fig. 24 Normalized In-Plane Reflected Distributions for $N_2$ - 915-percent Ar from 23°K Target**

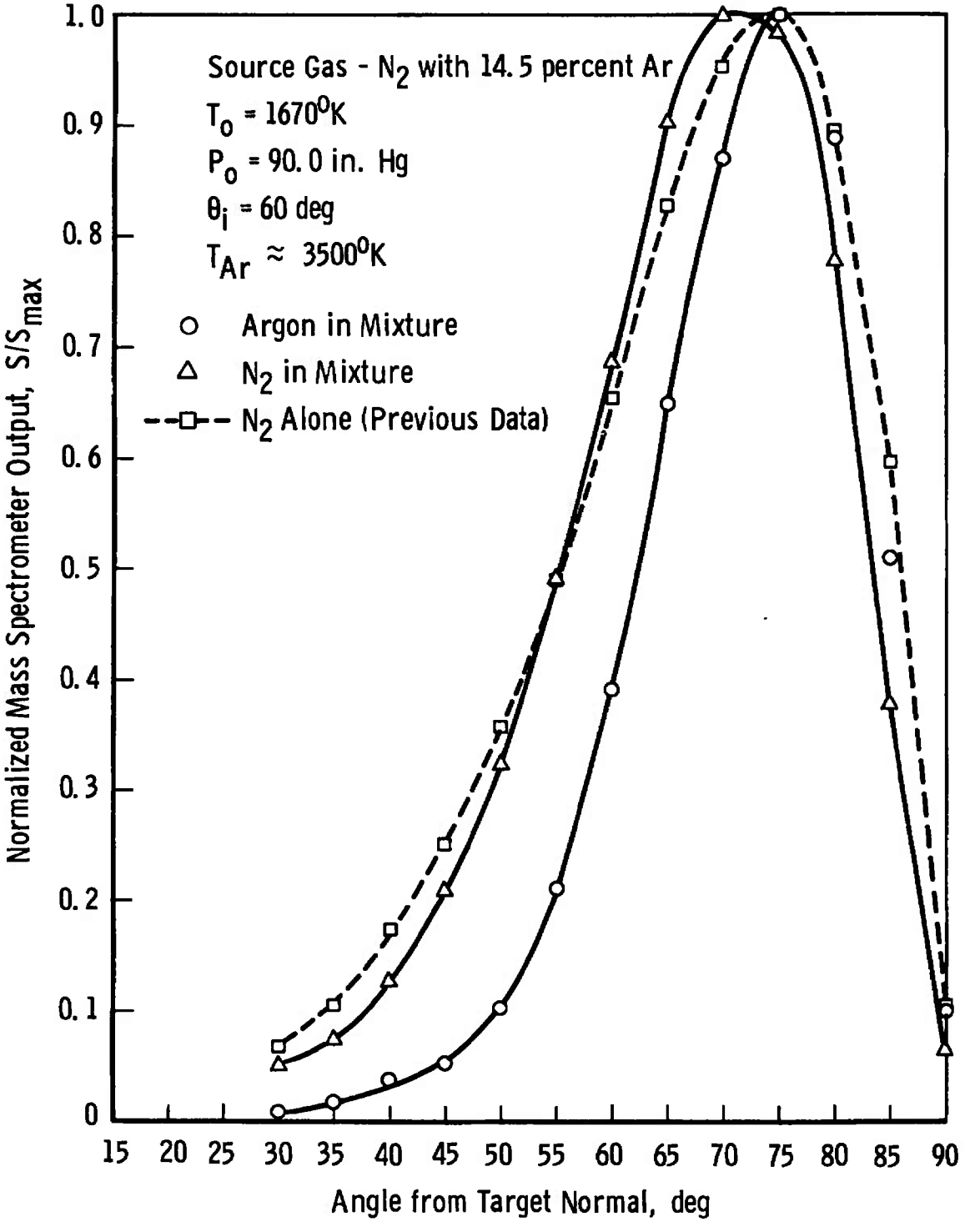


**Fig. 25 Normalized In-Plane Reflected Distributions for $N_2$ - 14.5-percent Ar from 23°K Target**

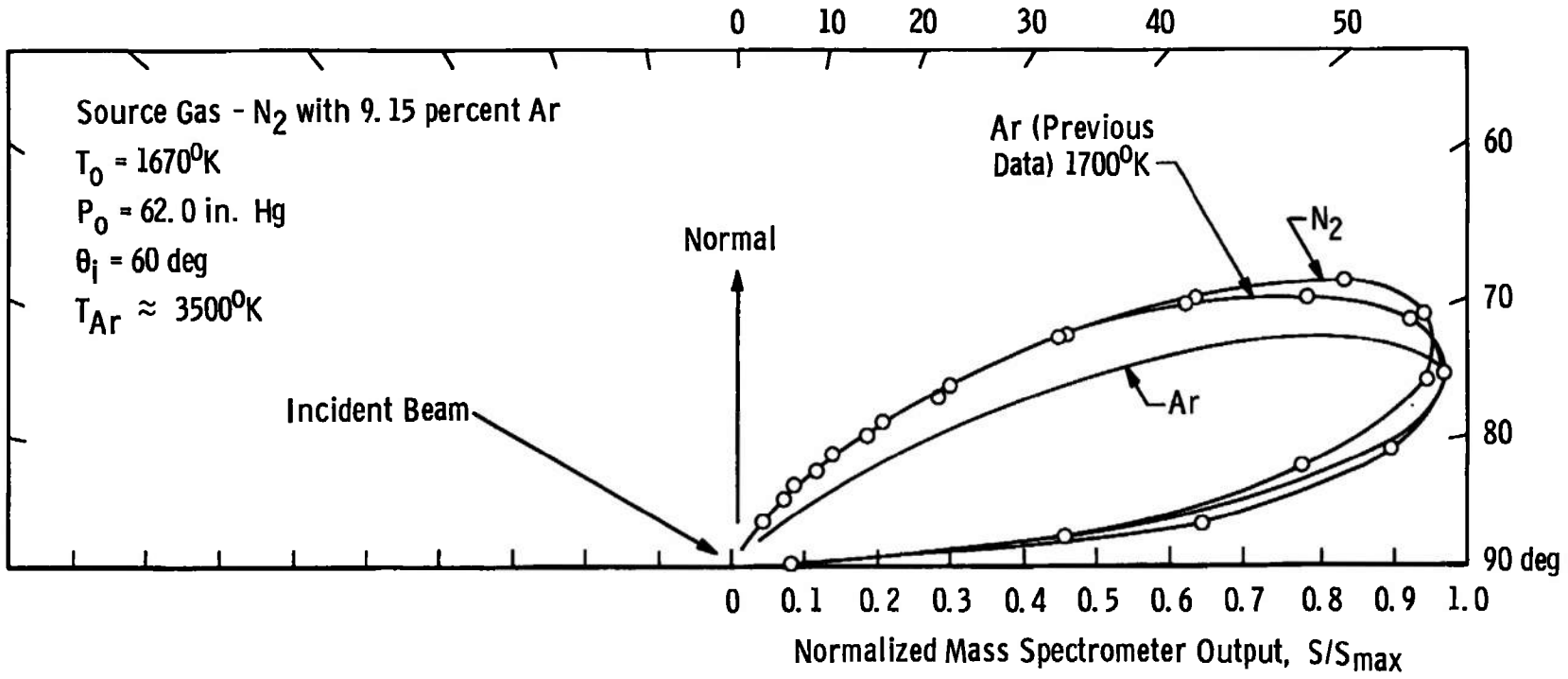


Fig. 26 Normalized In-Plane Reflected Distribution for $N_2$ - 9.15-percent Ar from 23°K Target (Polar)

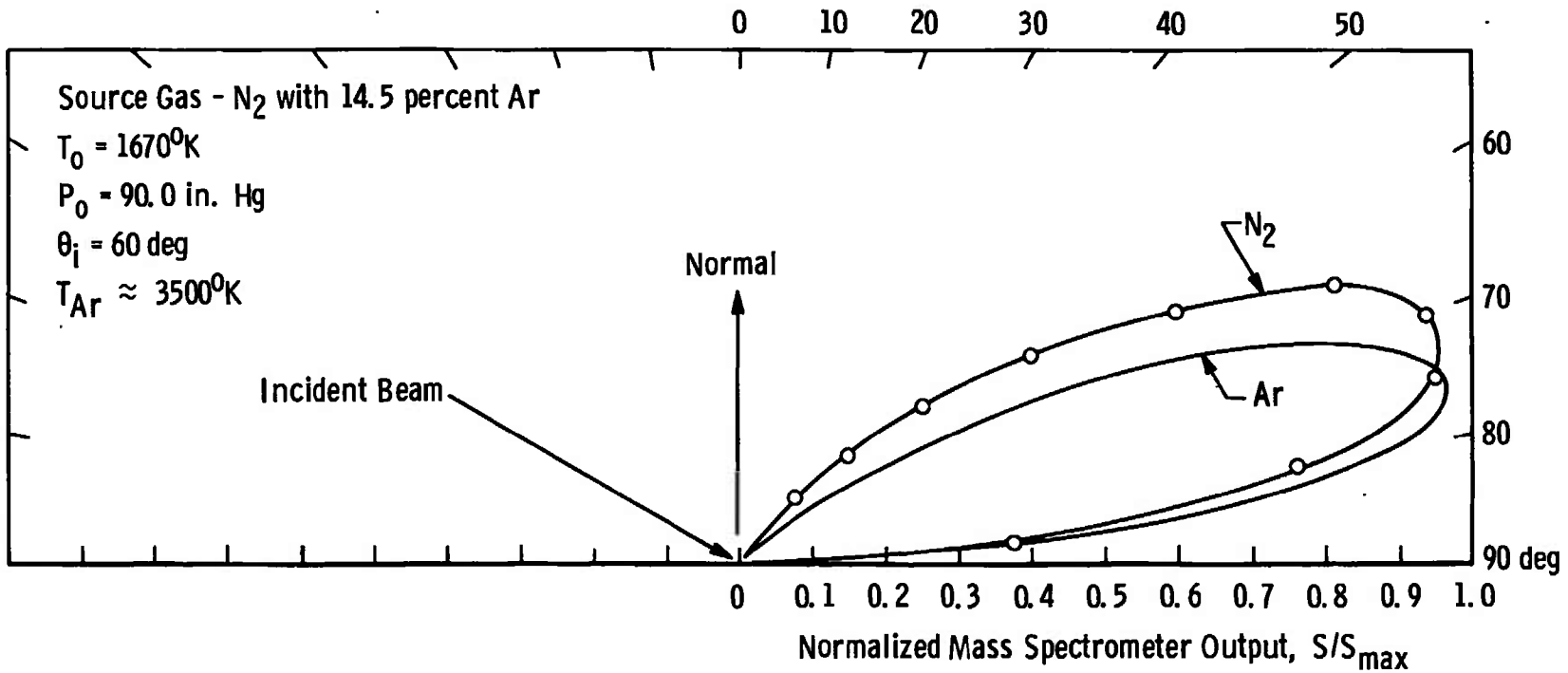


**Fig. 27 Normalized In-Plane Reflected Distribution for $N_2$ - 14.5-percent Ar from 23° K Target (Polar)**

UNCLASSIFIED
Security Classification

## DOCUMENT CONTROL DATA - R & D

*(Security classification of title, body of abstract and indexing annotation must be entered when the overall report is classified)*

1. ORIGINATING ACTIVITY *(Corporate author)*
Arnold Engineering Development Center
ARO, Inc., Operating Contractor
Arnold Air Force Station, Tennessee 37389

2a. REPORT SECURITY CLASSIFICATION
UNCLASSIFIED

2b. GROUP
N/A

3. REPORT TITLE
EXPERIMENTAL INVESTIGATION OF THE SCATTERING OF A NITROGEN AERODYNAMIC MOLECULAR BEAM FROM A SOLID NITROGEN SURFACE

4. DESCRIPTIVE NOTES *(Type of report and inclusive dates)*
Final Report December 1969 to January 1970

5. AUTHOR(S) *(First name, middle initial, last name)*
Frederick Arnold, M. R. Busby, and Ronald Dawbarn, ARO, Inc.

| 6. REPORT DATE | 7a. TOTAL NO. OF PAGES | 7b. NO. OF REFS |
|---|---|---|
| October 1970 | 51 | 17 |

| 8a. CONTRACT OR GRANT NO | 9a. ORIGINATOR'S REPORT NUMBER(S) |
|---|---|
| F40600-71-C-0002 | AEDC-TR-70-172 |
| b. PROJECT NO. 8951 | |
| c. Program Element 61102F | 9b. OTHER REPORT NO(S) *(Any other numbers that may be assigned this report)* ARO-VKF-TR-70-172 |
| d. | |

10. DISTRIBUTION STATEMENT
This document has been approved for public release and sale; its distribution is unlimited.

| 11. SUPPLEMENTARY NOTES | 12. SPONSORING MILITARY ACTIVITY |
|---|---|
| Available in DDC. | Arnold Engineering Development Center, Arnold Air Force Station, Tennessee 37389 |

13. ABSTRACT

An aerodynamic molecular beam and phase sensitive detection system were used to investigate the spatial distributions of nitrogen molecules scattered from solid nitrogen for (1) incident beam energies of 0.44 ev [source stagnation temperature ($T_o$) = 1440°K] to 0.88 ev ($T_o$ = 2760°K), (2) incident angles (with respect to surface normal) of 30 to 70 deg, and (3) a surface temperature of 23°K. Highly lobular reflected distributions centered 15 deg from the surface opposite the incident beam were observed with position and shape independent of incident energy and angle. The capture coefficient decreased sharply with increasing beam energy and incident angle from normal. A limited investigation of a nitrogen-argon mixture was also undertaken. The reflected spatial distributions for the components were similar to those observed for the individual pure gases. A seeding effect in the expansion was observed to accelerate the heavier gas. Transient effects were also investigated.

DD FORM 1 NOV 65 1473

UNCLASSIFIED
Security Classification

| 14. KEY WORDS | LINK A | | LINK B | | LINK C | |
|---|---|---|---|---|---|---|
| | ROLE | WT | ROLE | WT | ROLE | WT |
| solidified gases | | | | | | |
| cryogenics | | | | | | |
| molecular beams | | | | | | |
| rarefied gas dynamics | | | | | | |
| nitrogen | | | | | | |